Measurement and model-independent analysis of the x rays of muonic ^{150}Sm and ^{152}Sm*

Y. Yamazaki, E. B. Shera, and M. V. Hoehn
University of California, Los Alamos Scientific Laboratory, Los Alamos, New Mexico 87545

R. M. Steffen
Department of Physics, Purdue University, West Lafayette, Indiana 47907

(Received 31 March 1978)

Precision measurements, using a highly linear Ge(Li) spectrometer system, have been made of the muonic x-ray spectra of the ^{150}Sm and ^{152}Sm transitional nuclei. Equivalent Barrett nuclear charge radii for both of the isotopes have been determined. Generalized quadrupole moments of the charge distribution as probed by muonic atoms have been determined in a nearly model-independent way, and equivalent quadrupole radii for static and transitional quadrupole charge distributions of the 2^+ states have been determined by comparison with Coulomb excitation data. The isomer shift of the 2^+ state of ^{152}Sm was measured directly from the K x rays, while that of ^{150}Sm was determined from the observed nuclear γ ray. A phenomenological rotation-vibration-interaction model provides a satisfactory explanation for the observed quadrupole moment and isomer shift of the 2^+ state in ^{152}Sm.

[NUCLEAR STRUCTURE $^{150, 152}$Sm; measured muonic x-ray spectra; deduced monopole and quadrupole charge parameters, isotope and isomer shifts.]

I. INTRODUCTION

Accurate information about the multipole moments of the low-lying excited states of ^{150}Sm and ^{152}Sm is of particular interest, since these nuclei are in the transition region between spherical and deformed nuclei. The spectra of states of the transitional nuclei fit neither a vibrational nor a rotational pattern, although they exhibit some characteristics of both. The low-lying excited states of ^{150}Sm and ^{152}Sm (Ref. 1–4) can be classified into the "ground," "beta," "gamma," and octupole bands[1] as shown in Fig. 1.

Various models have been proposed which attempt a unified description of the transitional nuclei. The energy spectra of the low-lying states, $Q(2_g^+)$ and the known $B(E2)$ values of ^{152}Sm (Refs. 1, 4–13) can be reasonably well explained on the basis of the pairing-plus-quadrupole (PPQ) model, via either the Hartree-Bogoliubov calculation of Kumar[14,15] or the boson expansion calculation of Kishimoto and Tamura.[16] However, the former calculation fails to accurately predict the structure and the multipole moments of ^{150}Sm.[1-3,5,10,17]

It is well known that the negative muon can serve as a sensitive probe for the investigation of nuclear charge distributions. Nearly model-independent methods of analysis for the muonic x-ray data in terms of quadrupole and monopole charge distributions have been recently developed.[18-21] These methods, together with an increasingly complete understanding of higher-order quantum electrodynamical corrections of muonic-atom states,[22] now make it possible to extract from muonic x-ray data precise information about the electromagnetic structure of the nuclear ground state and in many cases, of nuclear excited states. The purpose of the present muonic x-ray study is to obtain accurate, model-independent data for the monopole and quadrupole charge moments of the 0_g^+ and 2_g^+ states of ^{150}Sm and ^{152}Sm.

II. MEASUREMENTS AND EXPERIMENTAL RESULTS

The muonic x-ray measurements were performed at the stopped-muon channel of the Clinton P. Anderson Meson Physics Facility at Los Alamos. Muons were stopped in an arrangement of three targets: 31 g of ^{152}Sm, 30 g of ^{150}Sm, and 25 g of ^{208}Pb. Muonic x rays from ^{208}Pb were used as energy and intensity calibration references. The isotopic purities of the Sm targets are listed in Table I. The spectra of all three targets were accumulated simultaneously to minimize the effect of instrumental instabilities using techniques similar to those described by Shera *et al.*[23] However, instead of a single common anticoincidence scintillation counter, three small anticoincidence counters, one for each individual target, were used to signal a stopped muon. This modification avoided excessive dead-time losses at the higher accelerator beam current which was available at the time of the present experiment. The electronics and computer-based data acquisition system were similar to that previously described[23] but with modifications to permit higher counting rates. The total muon stopping rate was typically 70 000 muons/s at an (average) accelerator beam current of about 50 μA.

The x rays were detected in a 60-cm^3 true-co-

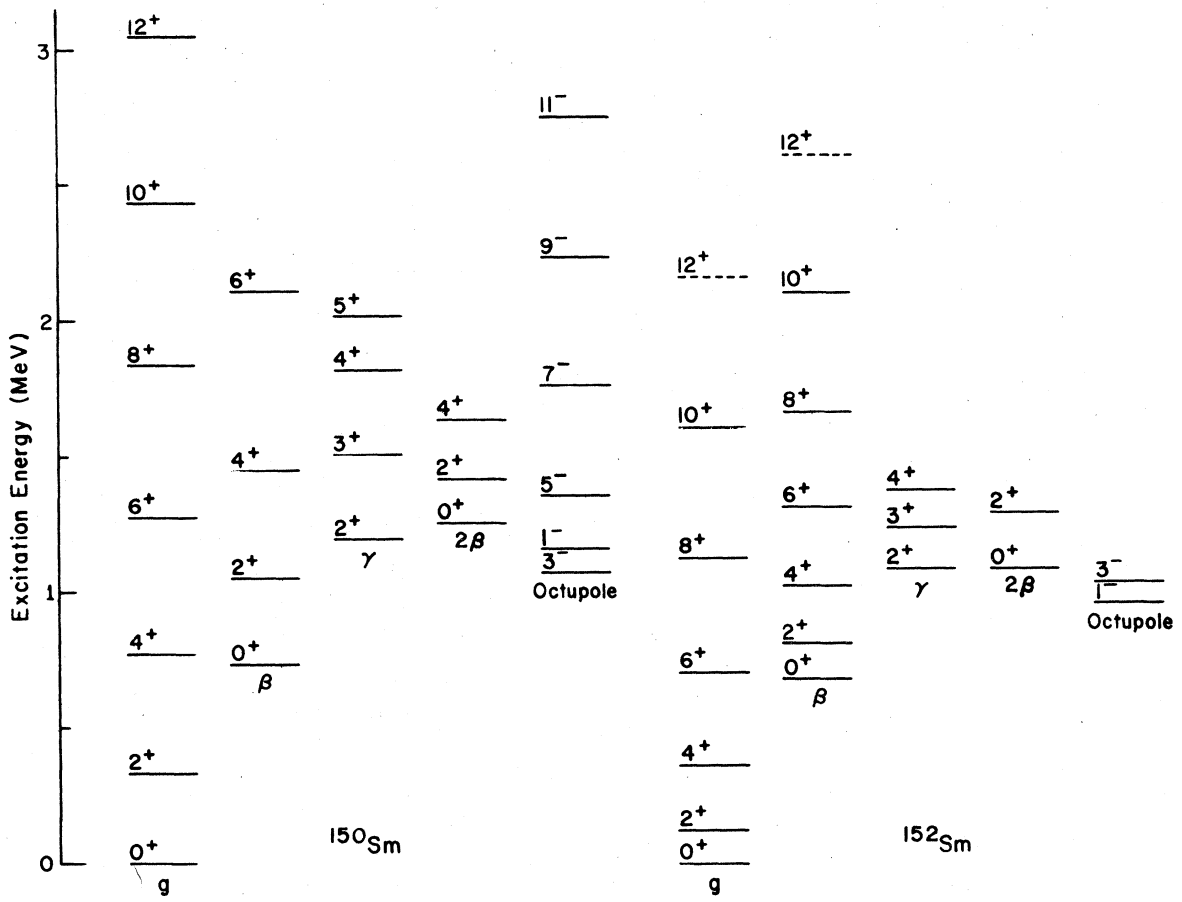

FIG. 1. Nuclear level schemes of ^{150}Sm and ^{152}Sm. Band assignments are identical to those of Ref. 1.

axial Ge(Li) detector. Ideally, the response of such a detector to monoenergetic radiation is a Gaussian pulse distribution. The natural shape of muonic x-ray lines, however, is Lorentzian. For the K and L x-ray transitions, the natural width of the lines is comparable to the detector resolution width and, hence, the observed pulse distribution is a Lorentzian convoluted with a Gaussian. In addition, distortions of the observed line shape near the base arise from incomplete charge collection in the detector and imperfections of the electronics (e.g., inexact pole-zero compensation and base-line restoration errors). In the present analysis the pulse distribution was approximated by adding exponential tails to a Gaussian-convoluted Lorentzian shape. This line shape plus a linear background was then fitted to the observed muonic x-ray spectra by the method of least squares. An example of a fitted spectrum is shown in Fig. 2.

TABLE I. Properties and isotopic compositions of the Sm targets.

Isotope chemical form	^{150}Sm SmO_2	^{152}Sm SmO_2
	Isotopic composition (%)	
^{144}Sm	0.05	0.02
^{147}Sm	0.39	0.20
^{148}Sm	0.47	0.19
^{149}Sm	1.70	0.29
^{150}Sm	95.48	0.24
^{152}Sm	1.46	98.29
^{154}Sm	0.45	0.76

The observed K and L transitions for ^{150}Sm and ^{152}Sm are shown in Figs. 3 and 4, respectively. The observed line energies and relative intensities are listed in Tables II and III. The energy calibration of the detector system was based on a linear interpolation from the observed positions of ^{208}Pb muonic x-ray lines, the energies of which were taken from Refs. 24 and 25. The total errors listed include the uncertainties associated with these calibration lines. The errors of the multiplet spacings are dominated by statistical errors since the uncertainty in the calibration function is relatively small for closely spaced lines. The listed energy values of the K x rays were obtained

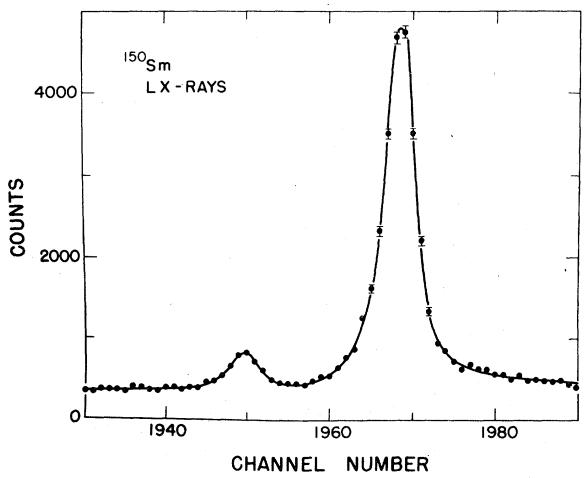

FIG. 2. Typical fitted line illustrating the Gaussian convoluted Lorentzian shape with exponential tails.

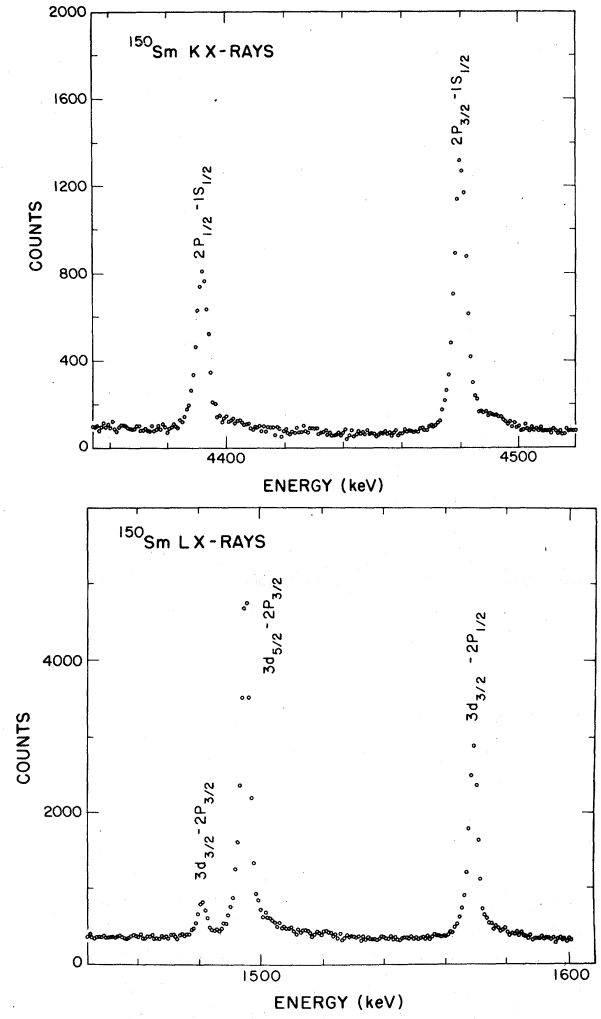

FIG. 3. Muonic K and L x-ray spectra of ^{150}Sm.

from a weighted average of the observed energies of the full-energy peaks, single-escape, and double-escape peaks.

The detector efficiency calibration was determined primarily from observation of the $^{14}N(n,\gamma)$ reaction spectrum (at high energies) and from standard radioactive sources (at low energies). The resulting efficiency calibration curve was slightly adjusted by imposing the constraint that $I_K = I_L = I_M$ where I_i represents the sum of the intensities of the muonic K, L, or M lines of ^{208}Pb.

III. ANALYSIS OF MUONIC SPECTRA

A. Model-independent analysis theory

A model-independent description of the effects of multipole charge distributions of a finite nucleus on the binding energies of muonic atoms has been discussed by Wagner *et al.*[21] This model-independent multipole method is a generalization of the method developed by Ford and Wills[18] and Barrett[19] for the model-independent determination of the monopole charge distribution. In the following discussion the approach of Wagner *et al.*[21] is used with some modifications that attempt to clarify the connection between the moments observed in muonic spectra, electron scattering, and the usual "point-nucleus" multipole moments (see, e.g., Bohr and Mottelson[26]).

The Hamiltonian of a free muonic atom can be written in the form

$$H = H_N + H_\mu + H^E_{N\mu} + H^M_{N\mu} + H', \tag{1}$$

where H_N is the free nuclear Hamiltonian with eigenstates $|\gamma IM\rangle$ and H_μ is the muon Hamiltonian with eigenstates $|\mu\rangle = |n\kappa(j)m\rangle$ which includes the static, Uehling,[27] and Källen-Sabry[28] potentials $V_0(r)$ (second- and fourth-order monopole vacuum polarization) produced by a spherically averaged reference nuclear charge distribution $\rho_0(r)$. The residual longitudinal electromagnetic interaction between the muon and nucleus is represented by $H^E_{N\mu}$. Interaction of the muon with the nuclear magnetic multipole moments is represented in Eq. (1) by the magnetic hyperfine interaction Hamiltonian $H^M_{N\mu}$. The term H' includes all other higher-order corrections (e.g., QED).

The Hamiltonian $H^E_{N\mu}$ can be expanded in terms of multipoles

$$H^E_{N\mu} = \sum_{L=0}^{\infty} H(\mathrm{EL}) - V_0. \tag{2}$$

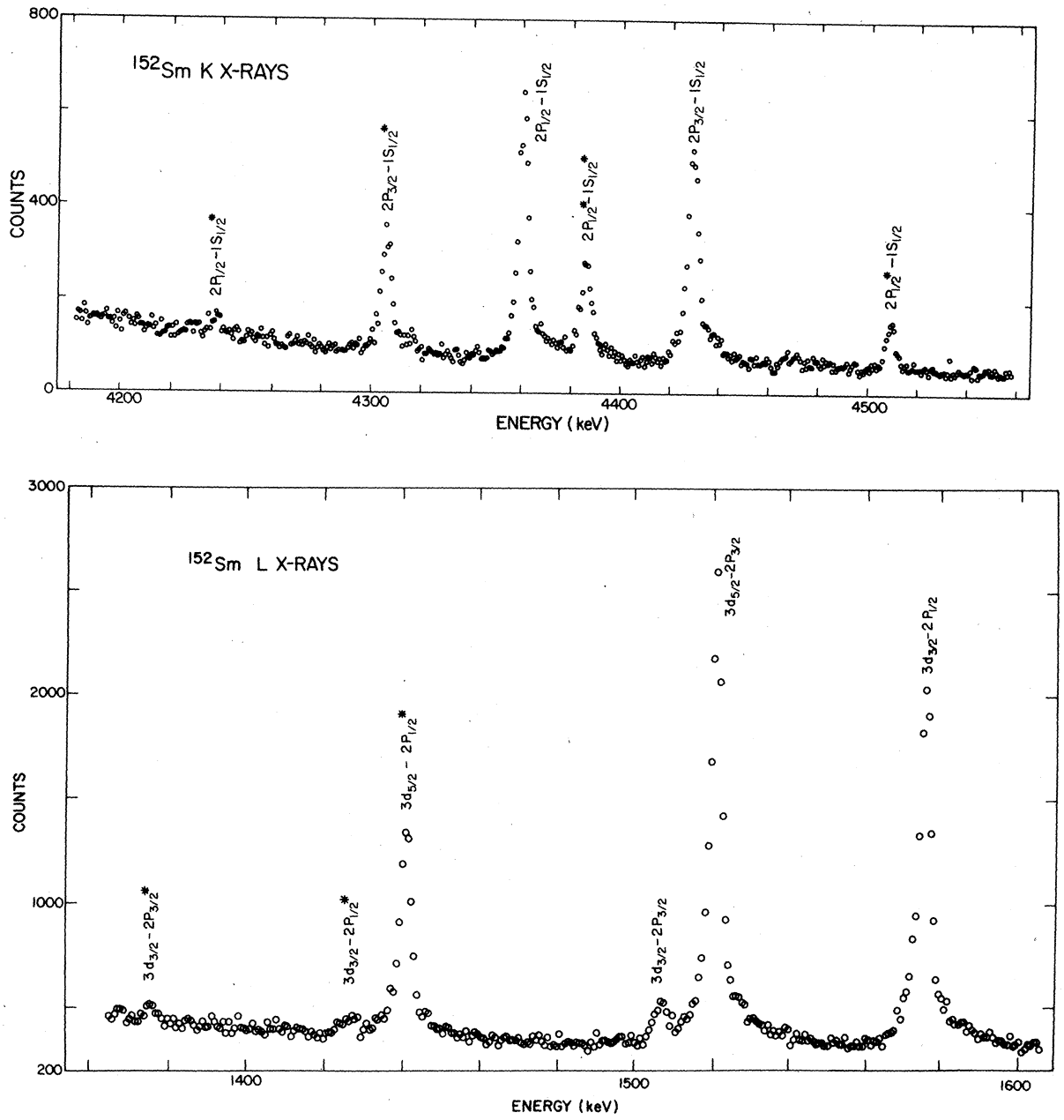

FIG. 4. Muonic K and L x-ray spectra of ^{152}Sm.

The operator $H(\mathrm{EL})$ of Eq. (2) can be expressed in the form

$$H(\mathrm{EL}) = -\frac{4\pi}{2L+1}\sum_{M=-L}^{L}\int d^3r_N e\rho(\vec{r}_N)\frac{r_<^L}{r_>^{L+1}} \times Y_{LM}(\Omega_N)Y^*_{LM}(\Omega_\mu), \quad (3)$$

where $\rho(\vec{r}_N)$ is the nuclear charge distribution operator. The 2^L-pole vacuum polarization is not included in this interaction Hamiltonian (see Sec. III C). The matrix elements of $H(\mathrm{EL})$ in the coupled muon-nuclear representation $|i\rangle = |\gamma I \otimes n\kappa; F\phi\rangle$ are given by

TABLE II. Measured and calculated x-ray energies and intensities for muonic ^{150}Sm. All of the observed or calculated transitions with energies greater than 700 keV and with intensities larger than 0.01 for $E>1100$ keV and 0.002 for $E<1100$ keV are listed. For transitions below 700 keV only resolved peaks are listed, although all of the unresolved peaks that were observed below 700 keV could be assigned. The intensities are normalized to the summed intensity of the $K\alpha$ x rays. Theoretical values are calculated assuming a deformed Fermi charge distribution with $c=5.855\,991$ fm, $a=0.556\,995$ fm, $\beta_2=0.231$, and $B(E2;0^+\rightarrow 2^+)=14\,744.3\ e^2\,\mathrm{fm}^4$. Other parameters used in the calculation are listed in Tables V, VII, and XIII. Comparison of the observed and calculated transition energies and intensities yields the following chi-squared values: $\chi^2_{\mathrm{Energy}}=4.65$ ($\chi^2_{\mathrm{Energy}}/14=0.33$), $\chi^2_{\mathrm{Intensity}}=14.4$ ($\chi^2_{\mathrm{Intensity}}/17=0.85$) where transitions involving $2s_{1/2}$ state are excluded and statistical errors are used.

	Energy (keV)					Intensity		
Transition	Experiment	Theory	Difference	Statistical error	Total error	Experiment	Theory	Error
K x rays								
$2p_{3/2}$-$1s_{1/2}$	4479.41	4479.39	+0.02	0.06	0.27	0.648	0.658	0.017
$2p_{1/2}$-$1s_{1/2}$	4391.33	4391.36	−0.03	0.07	0.28	0.352	0.342	0.029
L x rays								
$3d_{3/2}$-$2p_{1/2}$	1569.09	1569.18	−0.09	0.14	0.15	0.286	0.289	0.017
$3d_{5/2}$-$2p_{3/2}$	1495.32	1495.32	+0.00	0.10	0.11	0.482	0.508	0.021
$3d_{3/2}$-$2p_{3/2}$	1481.23	1481.15	+0.08	0.13	0.14	0.051	0.052	0.003
M x rays								
$4f_{5/2}$-$3d_{3/2}$	544.15	544.11	+0.04	0.08	0.09	0.314	0.280	0.029
$4f_{7/2}$-$3d_{5/2}$	532.90	532.91	−0.01	0.10	0.11	0.412	0.398	0.045
Weak x rays								
$3p_{3/2}$-$2s_{1/2}$	1026.98	1027.67	−0.69	0.12	0.15	0.017	0.011	0.002
$3p_{1/2}$-$2s_{1/2}$	Unresolved	1003.63						
$2s_{1/2}$-$2p_{3/2}$	470.75	470.15	+0.60	0.11	0.11	0.014		0.002
$4d_{3/2}$-$2p_{1/2}$	2107.15	2107.10	+0.05	0.15	0.16	0.022	0.024	0.004
$4d_{5/2}$-$2p_{3/2}$	2025.00	2025.02	−0.02	0.12	0.14	0.054	0.043	0.010
$9f_{5/2}$-$3d_{3/2}$	1091.52	1091.36	+0.16	0.35	0.36	0.003	0.002	0.002
$9f_{7/2}$-$3d_{5/2}$	Unresolved							
$8f_{5/2}$-$3d_{3/2}$	1055.84	1055.75	+0.09	0.52	0.52	0.004	0.002	0.002
$8f_{7/2}$-$3d_{5/2}$	1042.12	1041.95	+0.17	0.23	0.25	0.005	0.003	0.001
$7f_{5/2}$-$3d_{3/2}$	Unresolved	1003.70						
$7f_{7/2}$-$3d_{5/2}$	989.88	990.08	−0.20	0.36	0.37	0.005	0.007	0.002
$6f_{5/2}$-$3d_{3/2}$	923.19	923.33	−0.14	0.13	0.15	0.012	0.011	0.002
$6f_{7/2}$-$3d_{5/2}$	910.03	910.04	−0.01	0.16	0.17	0.015	0.015	0.003
$5f_{5/2}$-$3d_{3/2}$	789.87	789.85	+0.02	0.06	0.08	0.038	0.035	0.002
$5f_{7/2}$-$3d_{5/2}$	777.12	777.20	−0.08	0.09	0.10	0.053	0.050	0.004
γ ray								
2^+_g-0^+_g	336.64	333.95[a]		0.13	0.14	0.026	0.012	0.003
Unassigned	4954.94							
	1198.01							
	861.43							

[a] γ-ray energy in absence of muon.

$$\langle \gamma_2 I_2 \otimes n_2\kappa_2(j_2); F\phi \,|H(EL)|\, \gamma_1 I_1 \otimes n_1\kappa_1(j_1); F\phi\rangle = -(-1)^{F+I_1-1/2}\left(\frac{4\pi}{2L+1}\right)^{1/2}[(2j_1+1)(2j_2+1)]^{1/2}\begin{pmatrix} j_1 & j_2 & L \\ -\frac{1}{2} & \frac{1}{2} & 0\end{pmatrix}$$
$$\times \begin{Bmatrix} I_1 & j_1 & F \\ j_2 & I_2 & L\end{Bmatrix}\langle n_2\kappa_2 \,||e r^{-(L+1)}||\, n_1\kappa_1\rangle\langle \gamma_2 I_2 \,||\bar{M}^{n_2\kappa_2, n_1\kappa_1}(\mathrm{EL})||\, \gamma_1 I_1\rangle , \quad (4)$$

where

$$\langle n_2\kappa_2 \,||e r^{-(L+1)}||\, n_1\kappa_1\rangle = e\int_0^\infty \phi_L{}^{n_2\kappa_2, n_1\kappa_1}(r) r^2 dr .$$

The function $\phi_L^{n_2\kappa_2, n_1\kappa_1}(r)$ can be expressed in terms of the usual radial solution to the Dirac equation,

$$\phi_L^{n_2\kappa_2, n_1\kappa_1}(r) = \frac{1}{r^{L+1}}[f_{n_2\kappa_2}(r) f_{n_1\kappa_1}(r) + g_{n_2\kappa_2}(r) g_{n_1\kappa_1}(r)] . \quad (5)$$

The nuclear charge operator can be expressed

TABLE III. Measured and calculated x-ray energies and intensities for muonic ^{152}Sm. All of the observed or calculated transitions with energies greater than 500 keV and with intensities larger than 0.07 are listed except for unresolved peaks. No γ rays or unassignable transitions were observed. The states designated by $2p_{1/2}$, $2p_{3/2}$, $2p^*_{1/2}$, and $2p^*_{3/2}$ correspond with those of Fig. 5. The intensities are normalized to the summed intensities of $K\alpha$ x rays. Theoretical values are calculated assuming a deformed Fermi charge distribution with $c = 5.884\,929$ fm, $a = 0.544\,853$ fm, $\beta_2 = 0.284$, $\beta_4 = 0.07$, $B(E2; 0^+ \rightarrow 2^+) = 34\,572.2\ e^2\text{fm}^4$, and $Q(2^+) = -170.205\ e\,\text{fm}^2$. Other parameters used in the calculation are listed in Tables VI, VII, and IX. Comparison of the observed and calculated transition energies and intensities yields the following chi-squared values: $\chi^2_{\text{Energy}} = 8.47$ ($\chi^2_{\text{Energy}}/15 = 0.56$), $\chi^2_{\text{Intensity}} = 25.3$ ($\chi^2_{\text{Intensity}}/21 = 1.2$).

	Energy (keV)					Intensity		
Transition	Experiment	Theory	Difference	Statistical error	Total error	Experiment	Theory	Error
K x rays								
$2p^*_{1/2}$-$1s_{1/2}$	4508.77	4508.66	+0.11	0.13	0.29	0.063	0.065	0.005
$2p_{3/2}$-$1s_{1/2}$	4428.56	4428.57	−0.01	0.05	0.26	0.303	0.322	0.018
$2p^*_{1/2}$-$1s^*_{1/2}$	4385.56	4385.61	−0.05	0.11	0.28	0.133	0.122	0.008
$2p_{1/2}$-$1s_{1/2}$	4360.12	4360.15	−0.03	0.08	0.27	0.331	0.321	0.018
$2p_{3/2}$-$1s^*_{1/2}$	4305.55	4305.51	+0.04	0.10	0.28	0.156	0.154	0.009
$2p_{1/2}$-$1s^*_{1/2}$	4237.80	4237.80	−0.00	0.46	0.53	0.015	0.016	0.006
L x rays								
$3d_{3/2}$-$2p_{1/2}$	1575.60	1575.67	−0.07	0.10	0.12	0.272	0.242	0.016
$3d_{5/2}$-$2p_{3/2}$	1521.40	1521.43	−0.03	0.11	0.13	0.305	0.309	0.018
$3d_{3/2}$-$2p_{3/2}$	1507.41	1507.25	+0.16	0.17	0.18	0.031	0.033	0.003
$3d_{5/2}$-$2p^*_{1/2}$	1441.39	1441.33	+0.06	0.15	0.16	0.142	0.124	0.008
$3d_{3/2}$-$2p^*_{1/2}$	1427.51	1427.16	+0.35	0.45	0.45	0.013	0.011	0.002
$3d_{3/2}$-$2p^*_{3/2}$	1376.26	1376.45	−0.19	0.52	0.52	0.007	0.007	0.002
M x rays								
$4f_{5/2}$-$3d_{3/2}$	544.27	544.23	+0.04	0.09	0.10	0.297	0.279	0.030
$4f_{7/2}$-$3d_{5/2}$	533.02	533.01	+0.01	0.11	0.12	0.388	0.399	0.046
Weak x rays								
$3p_{3/2}$-$2s_{1/2}$	1022.30	1022.64	−0.34	0.23	0.25	0.018	0.011	0.003
$2s_{1/2}$-$2p_{3/2}$	500.83	500.57	+0.26	0.19	0.20	0.010		0.002
$4d_{3/2}$-$2p_{1/2}$	2113.76	2113.71	+0.05	0.16	0.17	0.022	0.023	0.003
$4d_{5/2}$-$2p_{3/2}$	2051.55	2051.24	+0.31	0.18	0.19	0.033	0.028	0.004
$4d_{5/2}$-$2p^*_{1/2}$	1970.94	1971.13	−0.19	0.37	0.38	0.015	0.014	0.003
$6f_{5/2}$-$3d_{3/2}$	923.23	923.44	−0.21	0.28	0.30	0.008	0.011	0.002
$6f_{7/2}$-$3d_{5/2}$	910.03	910.15	−0.12	0.43	0.44	0.007	0.015	0.003
$5f_{5/2}$-$3d_{3/2}$	789.91	789.96	−0.05	0.09	0.11	0.037	0.036	0.003
$5f_{7/2}$-$3d_{5/2}$	777.23	777.31	−0.08	0.13	0.15	0.052	0.051	0.005

in the form

$$\rho(\vec{r}_N) = \sum_i e_i \delta(\vec{r}_N - \vec{r}_i)$$

$$= \sum_i e_i \frac{\delta(r_N - r_i)}{r_N^2} \sum_{LM} Y^*_{LM}(\Omega_N) Y_{LM}(\Omega_i), \qquad (6)$$

where the sum extends over all nuclear constituents (e.g., nucleons, pions) of charge e_i. The vector $\vec{r}_i$ is an internal position vector on which the nuclear wave functions depend, while $\vec{r}_N$ is a macroscopic position vector. Since the interaction $H^E_{N_\mu}$ can be expanded in multipoles [see Eq. (2)], it is convenient to introduce the radial multipole charge-density operator

$$\rho_{LM}(r_N) = \int d\Omega_N \rho(\vec{r}_N) Y_{LM}(\Omega_N)$$

$$= \sum_i e_i \frac{\delta(r_N - r_i)}{r_N^2} Y_{LM}(\Omega_i). \qquad (7)$$

The matrix element of $\rho_{LM}(r_N)$ is given by

$$\langle \gamma_2 I_2 M_2 | \rho_{LM}(r_N) | \gamma_1 I_1 M_1 \rangle = (-1)^{I_2 - M_2} \begin{pmatrix} I_2 & L & I_1 \\ -M_2 & M & M_1 \end{pmatrix} \langle \gamma_2 I_2 || \rho_L(r_N) || \gamma_1 I_1 \rangle , \qquad (8)$$

where $\langle \gamma_2 I_2 || \rho_L(r_N) || \gamma_1 I_1 \rangle$ is the characteristic observable of the radial distribution of the nuclear static or transition 2^L-pole charge.

Continuing the development of Eq. (4), we define generalized (reduced) multipole moments by

$$\langle \gamma_2 I_2 || \bar{M}^{n_2\kappa_2, n_1\kappa_1}(\mathrm{EL}) || \gamma_1 I_1 \rangle = \int_0^\infty r_N^2 \, dr_N \langle \gamma_2 I_2 || \rho_L(r_N) || \gamma_1 I_1 \rangle S_L^{n_2\kappa_2, n_1\kappa_1}(r_N) , \qquad (9)$$

where $S_L^{n_2\kappa_2, n_1\kappa_1}(r_N)$ is a weighting function that depends on the radial dependence of the extranuclear

potential. In the case of muonic hyperfine structure interactions, $S_L^{n_2\kappa_2,n_1\kappa_1}(r_N)$ is given by

$$S_L^{n_2\kappa_2,n_1\kappa_1}(r_N)=r_N^L\left[\int_0^{r_N}\phi_L^{n_2\kappa_2,n_1\kappa_1}(r)\left(\frac{r}{r_N}\right)^{2L+1}r^2dr+\int_{r_N}^{\infty}\phi_L^{n_2\kappa_2,n_1\kappa_1}(r)r^2dr\right]\times\left[\int_0^{\infty}\phi_L^{n_2\kappa_2,n_1\kappa_1}(r)r^2dr\right]^{-1}. \quad (10)$$

Since the observed energy splittings of the muonic atom states are given by the matrix elements of Eq. (4), the generalized multipole moments of Eq. (9) are the characteristic observables of the nuclear charge distribution as revealed by muonic x-ray spectra. Note that for $r\to 0$ (point nucleus), the weighting function $S_L^{n_2\kappa_2,n_1\kappa_1}(r)$ reduces to $S_L^{n_2\kappa_2,n_1\kappa_1}(r)=r^L$. In that case the radial integral [Eq. (9)] is identical to the conventional 2^L-pole moment (as defined, for example, by Bohr and Mottelson[26])

$$\langle\gamma_2 I_2\,||M(\mathrm{EL})||\gamma_1 I_1\rangle=\int_0^{\infty}r_N^{L+2}dr_N\langle\gamma_2 I_2\,||\rho_L(r_N)||\gamma_1 I_1\rangle. \quad (11)$$

These conventional moments are related to the quadrupole moment and reduced transition probability by

$$Q(\gamma I)=\left(\frac{16\pi}{5}\right)^{1/2}\begin{pmatrix} I & 2 & I\\ -I & 0 & I\end{pmatrix}\langle\gamma I\,||M(E2)||\gamma I\rangle, \quad (12a)$$

$$B(\mathrm{EL};\gamma_1 I_1\to\gamma_2 I_2)=\frac{1}{2I_1+1}|\langle\gamma_2 I_2\,||M(\mathrm{EL})||\gamma_1 I_1\rangle|^2. \quad (12b)$$

As indicated by Wagner *et al.*,[21] the weighting function $S_L^{n_2\kappa_2,n_1\kappa_1}(r)$ for a particular muon transition can be approximated within the range of overlap of the muon and nuclear wave functions by the expression

$$S_L^{n_2\kappa_2,n_1\kappa_1}(r)=r^L(A+Br^m e^{-\alpha r}), \quad (13)$$

where m and α depend on $n_1\kappa_1$ and $n_2\kappa_2$. Owing to the modified expansion of Eq. (4) used in the present treatment, as compared with that of Ref. 21, the numerical values of the coefficients A and B in Eq. (13) are different from the expressions in Ref. 21 by the factor $\langle n_2\kappa_2\,||r^{-(L+1)}||n_1\kappa_1\rangle$. To clarify the relationship between the muon-determined moments and the conventional point 2^L-pole moments, we note that the reduced nuclear matrix element of Eq. (9) can be expressed as

$$\langle\gamma_2 I_2\,||\bar{M}^{n_2\kappa_2,n_1\kappa_1}(\mathrm{EL})||\gamma_1 I_1\rangle=\langle\gamma_2 I_2\,||M(\mathrm{EL})||\gamma_1 I_1\rangle\times\int_0^{\infty}F_L(r)S_L^{n_2\kappa_2,n_1\kappa_1}(r)r^2dr. \quad (14)$$

$F_L(r)$ contains the radial dependence of the multipole charge density and can be computed, for example, from a particular nuclear model.

As mentioned by Wagner *et al.*,[21] the concept of generalized multipole moments can be applied to other processes in which the interaction of the nuclear charge distribution with the incoming particle x is dominated by the longitudinal electromagnetic interaction Hamiltonian $H(\mathrm{EL})$, e.g., electron scattering processes and Coulomb excitation. The factor $\langle n_2\kappa_2\,||r^{-(L+1)}||n_1\kappa_1\rangle$ in Eq. (4) can then be replaced by the Mott scattering factor and the process can be characterized by the generalized multipole moments $\langle\gamma_2 I_2\,||\bar{M}^x(\mathrm{EL})||\gamma_1 I_1\rangle$ with a weighting function $S_L^x(r)$ that depends on the particular process involved. In electron scattering measurements, the weighting function in the plane-wave Born approximation is given by

$$S_L^{e,e'}(r)=j_L(qr), \quad (15)$$

where $j_L(qr)$ is a spherical Bessel function, and q is the momentum transfer. In Coulomb excitation measurements with low-momentum transfer (long wave-length limit), the weighting function becomes

$$S_L^{CE}(r)=r^L, \quad (16)$$

indicating that such measurements yield point-nucleus moments.

These point-nucleus moments can be used in combination with the muon-determined moments to obtain a characteristic property of the radial distribution of the multipole charge distribution. In analogy to the equivalent Barrett radius R_k for the monopole distribution, Wagner *et al.*[21] have defined the equivalent multipole radius R_m,

$$\langle\gamma_2 I_2\,||\bar{M}^{n_2\kappa_2,n_1\kappa_1}(\mathrm{EL})||\gamma_1 I_1\rangle=(A+BR_m^m e^{-\alpha R_m})\times\langle\gamma_2 I_2\,||M(\mathrm{EL})||\gamma_1 I_1\rangle, \quad (17)$$

where R_m can be interpreted as the radius of a δ-function representation of $\langle\gamma_2 I_2\,||\rho_L(r)||\gamma_1 I_1\rangle$. R_m is a single integral parameter which characterizes the radial distribution of the multipole charge distribution.

Another quantity whose value is characteristic of a particular nuclear model is the ratio of static to transitional moments,

$$R(22,02)=-\left(\frac{7}{10}\right)^{1/2}\frac{\langle 2_g^+||\overline{M}^{n_2\kappa_2,n_1\kappa_1}(E2)||2_g^+\rangle}{|\langle 2_g^+||\overline{M}^{n_2\kappa_2,n_1\kappa_1}(E2)||0_g^+\rangle|}. \quad (18)$$

This ratio is derived entirely from the analysis of the muonic x-ray spectra and, therefore, it can often be determined more precisely than quantities, such as R_m, which depend in part upon the results of other types of measurements. The pure rotational model value of $R(22,02)$ is ± 1, while the pure vibrational model value is $R(22,02)=0$. Using Eq. (17) we can express the ratio R in the form

$$R(22,02)\cong-\left(\frac{7}{10}\right)^{1/2}\frac{\langle 2_g^+||M(E2)||2_g^+\rangle}{|\langle 2_g^+||M(E2)||0_g^+\rangle|}\left(1+\frac{\delta R_m}{C_R}\right), \quad (19)$$

where δR_m is the difference between the equivalent static quadrupole radius R_m^{22} and the equivalent transition quadrupole radius R_m^{02}. The sensitivity $C_R=\partial\delta R_m/\partial R(22,02)$ in Eq. (19) is given by

$$C_R=\frac{\partial(\delta R_m)}{\partial R(22,02)}=\frac{A+BR_m^m e^{-\alpha R_m}}{BR_m^m e^{-\alpha R_m}(mR_m^{-1}-\alpha)}. \quad (20)$$

B. General considerations and charge distribution models

In the preceding section general methods which are useful in the analysis of muonic atom data were discussed. We will now show how these methods have been applied to the particular cases of ^{150}Sm and ^{152}Sm.

The effects of the charge distribution of a finite nucleus are large enough to be observed only if there is an appreciable overlap of the muon wave function with the nuclear charge distribution. Thus, in general, only muon states with a small principal quantum number are useful in the determination of nuclear properties. Also, as a first approximation, the participation of higher excited nuclear states in the muon-nuclear hyperfine interaction can be neglected. Hence, to obtain the eigenvalues of the mixed muon-nuclear system, it is convenient to diagonalize the Hamiltonian $H_{N\mu}^E$ [see Eq. (4)] in a limited space of muon and nuclear states. Contributions from muon and nuclear states outside this limited space can be treated as corrections to the muon binding energies (see Sec. III C).

In this work the interest is concentrated on the static and dynamic quadrupole hyperfine interaction, which is represented by $H(E2)$. In the limited space consisting of the muonic $2p_{1/2}$ and $2p_{3/2}$ states and the nuclear ground and first excited 2^+ states (see Fig. 5), the $2p$ hyperfine splittings are entirely determined by the "unperturbed" $2p_{1/2}$-$2p_{3/2}$ fine-structure splitting and by the generalized quadrupole moments

$$\langle 2^+||\overline{M}^{2p_{1/2},2p_{3/2}}(E2)||0^+\rangle, \quad (21a)$$

$$\langle 2^+||\overline{M}^{2p_{1/2},2p_{3/2}}(E2)||2^+\rangle, \quad (21b)$$

$$\langle 2^+||\overline{M}^{2p_{3/2},2p_{3/2}}(E2)||0^+\rangle, \quad (21c)$$

$$\langle 2^+||\overline{M}^{2p_{3/2},2p_{3/2}}(E2)||2^+\rangle. \quad (21d)$$

The energy of the 2^+ state (corrected for any possible isomer shift) is assumed to be known or derivable from other measurements. It should be recognized that an independent determination of the fine-structure splitting and the four quadrupole moments from the observed $2p$ hyperfine splittings is a practical impossibility with present experimental techniques. However, as pointed out by Wagner *et al.*,[21] because of the similarity of the muon-generated quadrupole transition potentials, the weighting functions $S_L^{n_2\kappa_2,n_1\kappa_1}(r)$ involving the $(2p_{1/2}$-$2p_{3/2})$ and $(2p_{3/2}$-$2p_{3/2})$ muon states are nearly identical and can be approximated by Eq. (13) using the same values of m and α (the quantitative similarity of the $2p$ quadrupole transition potentials will be discussed below). Hence, the four matrix elements mentioned above can be represented by only two independent variables, here chosen to be $\langle 2^+||\overline{M}^{2p_{1/2},2p_{3/2}}(E2)||0^+\rangle$ and $\langle 2^+||\overline{M}^{2p_{1/2},2p_{3/2}}(E2)||2^+\rangle$. In addition, the "unperturbed" $2p_{1/2}$-$2p_{3/2}$ fine-structure splitting is insensitive to the form of the monopole charge distribution for given $2p_{1/2}$ and $1s_{1/2}$ binding energies and, therefore, this splitting can be calculated in a relatively model-independent way.

To obtain approximate nuclear charge parameters for ^{150,152}Sm so that, for example, the "unperturbed" $2p_{1/2}$-$2p_{3/2}$ fine-structure splitting can be computed, it is convenient to assume a specific form for the nuclear charge distribution and adjust the parameters of that distribution until the $1s_{1/2}$ and unperturbed $2p_{1/2}$ muonic binding energies are reproduced. The use of a specific charge model also provides a convenient method by which the model-independent monopole charge radii R_k can be computed from the observed spectra. In the present analysis a deformed Fermi function

$$\rho^{\mathrm{DF}}(\vec{r})=\rho_0\left[1+\exp\left(\frac{r-c[1+\beta_2 Y_{20}(\Omega)+\beta_4 Y_{40}(\Omega)]}{a}\right)\right]^{-1} \quad (22)$$

was used to represent the nuclear charge distribution.

To explore the invariance of the fine-structure splitting to the charge distribution, several modified "Fermi-type" model distributions of the form

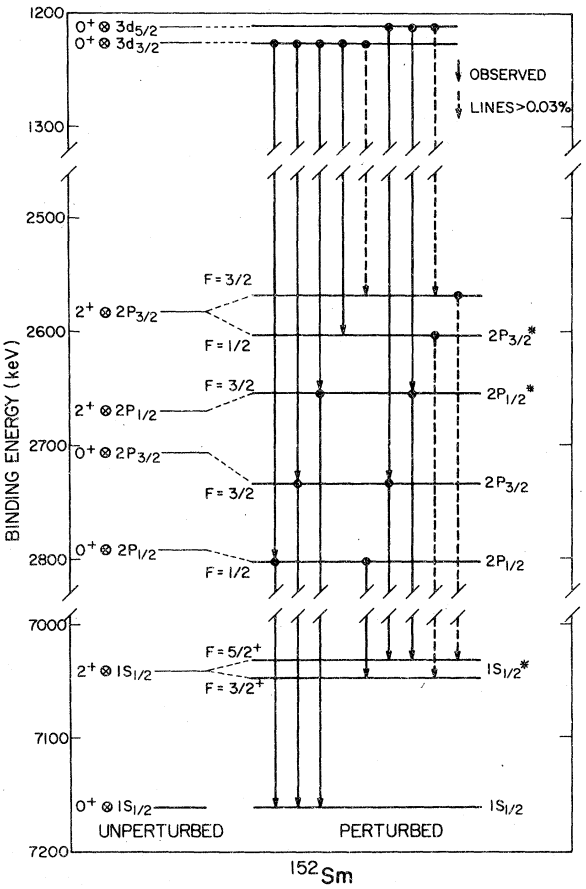

FIG. 5. Muonic transitions for ^{152}Sm. Observed transitions are indicated by solid lines, while unobserved transitions with calculated intensities greater than 0.03 percent are indicated by dashed lines.

$$\rho^{\mathrm{F}}(r)=\rho_0\frac{1+w(r/c)^2+D(1+r/c)^P\cos(br+d)}{\{1+\exp[(r-c)/a]\}^n}, \tag{23}$$

and an harmonic oscillator distribution of the form

$$\rho^{\mathrm{HO}}(r)=\rho_0[1+w(r/a)^2]\exp[-(r/a)^2] \tag{24}$$

were used. With various fixed values of w, n, D, P, b, and d, the parameters c and a were adjusted to reproduce the $3d_{3/2}\rightarrow 2p_{1/2}$ and $2p_{1/2}\rightarrow 1s_{1/2}$ muonic transition energies for ^{150}Sm. Although the resulting distributions were rather different (see Fig. 6), the calculated $2p_{1/2}$-$2p_{3/2}$ fine-structure splitting energies, listed in Table IV, were nearly identical to that calculated using a reference deformed Fermi charge distribution.

A deformed Fermi charge distribution was also used as the basis from which to derive a reasonable model for the quadrupole nuclear charge distribution so that the generalized muonic multipole moments $\langle\gamma_2 I_2||\overline{M}^{n_2\kappa_2,n_1\kappa_1}(E2)||\gamma_1 I_1\rangle$ could be expressed in terms of the conventional quadrupole matrix elements, i.e., quadrupole moments $Q(I)$ and $B(E2)$ values. The transition matrix elements obtained in this way obviously depend upon the radial dependence of the particular charge model employed, as is evident from Eqs. (9) and (14). The distribution $\rho^{\mathrm{DF}}(\vec{r})$ was used to calculate the radial dependence of the quadrupole charge-density operator [see Eq. (14)] by means of the following ansatz:

$$F_2^{\mathrm{DF}}(r)=\frac{\int\rho^{\mathrm{DF}}(\vec{r})Y_{20}(\Omega)d\Omega}{\int\rho^{\mathrm{DF}}(\vec{r})Y_{20}(\Omega)r^2d^3r}. \tag{25}$$

By representing the charge distribution as a deformed Fermi function and by using the ansatz of Eq. (25), we have implied a specific value X_{DF} for the ratio of the generalized moments involving the $(2p_{1/2}$-$2p_{3/2})$ and $(2p_{3/2}$-$2p_{3/2})$ muon states

$$X=\frac{\langle\gamma_2 I_2||\overline{M}^{2p_{1/2},2p_{3/2}}(E2)||\gamma_1 I_1\rangle}{\langle\gamma_2 I_2||\overline{M}^{2p_{3/2},2p_{3/2}}(E2)||\gamma_1 I_1\rangle}. \tag{26}$$

In order to explore the model dependence introduced by the specific value X_{DF}, we computed the value $X(R_m)$ of this ratio for a δ-function quadrupole charge distribution $F_2^{\delta}(r)=\delta(r-R_m)/r^4$. Figure 7 shows the ratio $X(R_m)/X_{\mathrm{DF}}$ plotted as a function of the quadrupole radius R_m. As is evident from the figure, the deviation of $X(R_m)$ from X_{DF} is less than 1% in the range $0<R_m<10$ fm, and more significantly, the ratio $X(R_m)/X_{\mathrm{DF}}$ varies less than 0.3% in the region $6<R_m<8$ fm.

Although the experimental results can be quoted in terms of the conventional moments, it is evident that the moments

$$\langle\gamma_2 I_2||\overline{M}^{2p_{1/2},2p_{3/2}}(E2)||\gamma_1 I_1\rangle,$$

the quantities actually measured in muonic x-ray studies, are better quantities with which to compare theoretical calculations since they avoid the model dependence of the $B(E2)$ and quadrupole moment values derived from a specific assumed charge distribution. However, for convenience in comparing the present results with previous measurements, both model-dependent and model-independent types of parameters were derived from the muonic data for ^{150}Sm and ^{152}Sm, as will be discussed in the following section.

C. Corrections to the energies of muonic states

1. Higher-order quantum electrodynamical and related corrections

The second-order $\alpha(Z\alpha)$ and fourth-order $\alpha^2(Z\alpha)$ monopole vacuum polarization corrections have been included as a potential[27-29] in the relativistic Hamiltonian which was used in the solution of the

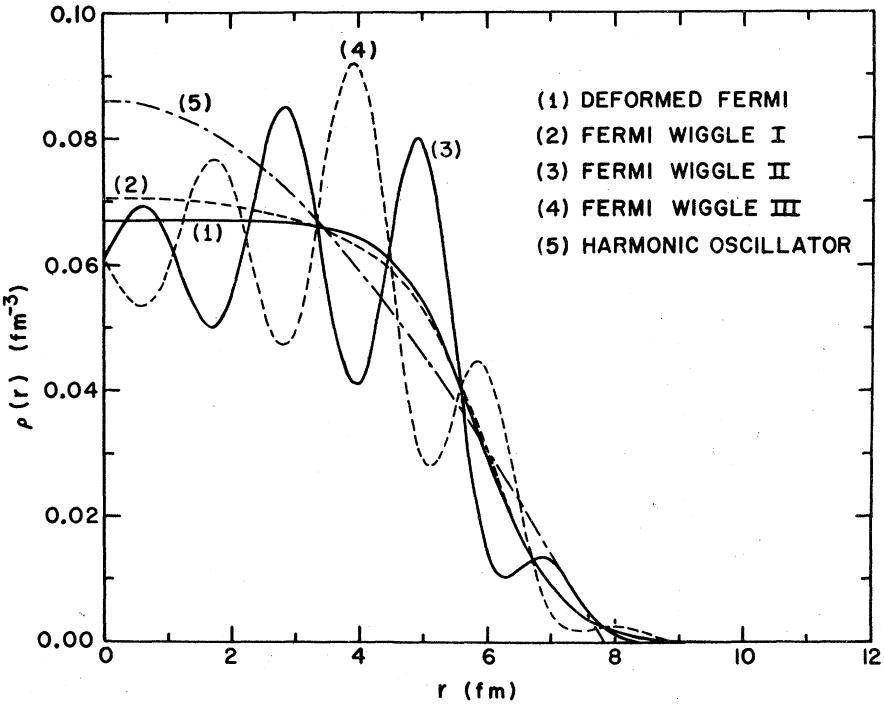

FIG. 6. Five charge distributions which yield the same $3d_{3/2}$-$2p_{1/2}$ and $2p_{1/2}$-$1s_{1/2}$ ^{150}Sm transition energies.

Dirac equation for the muonic atom. It is of interest to note that the inclusion of the monopole vacuum polarization potentials caused a 1% increase in the radial integrals involved in computing the multipole moments

$$\langle \gamma_2 I_2 || \overline{M}^{2p_{1/2}, 2p_{3/2}}(E2) || \gamma_1 I_1 \rangle .$$

The correction for quadrupole vacuum polarization (QVP), which was computed using the method of McKinley,[30] increased the $E2$ matrix elements by about 0.4%. The vacuum polarization correction of order $\alpha(Z\alpha)^{n\geq 3}$ and the vertex corrections which make up the so-called Lamb shift, as well as the relativistic recoil and electron screening correc-

TABLE IV. Comparison of results from different charge distributions. Parameters c and a (a and w in the harmonic-oscillator case) are fitted to the muonic $3d_{3/2}$-$2p_{1/2}$ and $2p_{1/2}$-$1s_{1/2}$ transition energies of ^{150}Sm. Corrections used in the calculation are listed in Table V. The results of the unperturbed $2p_{1/2}$-$2p_{3/2}$ fine-structure splitting include no dynamic $E2$ effect.

	Deformed Fermi	Fermi with wiggle I	Fermi with wiggle II	Fermi with wiggle III	Harmonic oscillator
Parameters c (fm)	5.855 991	6.075 740	5.864 558	5.854 106	···
a (fm)	0.556 995	0.590 421	0.792 515	0.785 134	15.021 133
w	···	−0.2	0.5	0.5	−3.666 527
β	0.231	···	···	···	···
n		1.0	1.5	1.5	
D		0	0.1	−0.1	
P		0	3.0	3.0	
b (fm^{-1})		0	2.8	2.8	
d		0	−1.5	−1.5	
Unperturbed					
$2p_{1/2}$-$2p_{3/2}$ splitting (keV)	86.976	86.974	86.980	86.977	86.961
$3p_{3/2}$-$2s_{1/2}$ energy (keV)	1027.672	1027.686	1027.650	1027.669	1027.782
$2s_{1/2}$-$2p_{3/2}$ energy (keV)	470.146	470.137	470.161	470.148	470.058
$\langle r^2 \rangle^{1/2}$ (fm)	5.0470	5.0467	5.0475	5.0470	5.0459

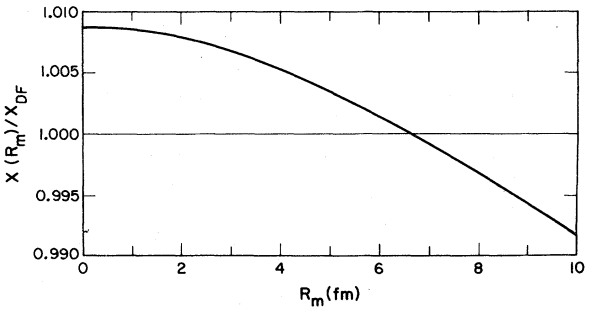

FIG. 7. Ratio $X(R_m)/X_{DF}$ as a function of the equivalent quadrupole radius R_m The figure illustrates the model dependence of the ratio X introduced by representing the charge distribution as a deformed Fermi model.

tions were computed by the methods of Ref. 22. Values of the various higher-order QED corrections for the states of muonic ^{150}Sm and ^{152}Sm are summarized in Tables V and VI, respectively. The estimated uncertainty of these corrections is much smaller than the experimental errors.[22]

2. *Nuclear polarization corrections*

The interaction Hamiltonian $H(E2)$ was diagonalized in only a limited subspace $|i_l>$ of the complete space that is spanned by the eigenstates $|i>$ of the "unperturbed" Hamiltonian $H_0=H_N+H_\mu$. The energy corrections to the eigenstates $|a>$ of the total Hamiltonian $H=H_0+H(E2)$ which are caused by the neglect of the states $|i_r>$ outside the "limited space" are defined as nuclear polarization corrections. In second-order perturbation theory the resulting energy shift of the state $|a>$ of the muonic atom is given by[31]

$$\Delta E_a = \sum_{l,l'=1}^{k} \langle a|i_l\rangle \left(\sum_{L=0}^{\infty} \Delta E_{l,l'}^{(L)}\right) \langle i_{l'}|a\rangle , \qquad (27)$$

where

$$\Delta E_{l,l'}^{(L)} = \sum_{r=k+1}^{\infty} \frac{\langle i_l|H(\mathrm{EL})|i_r\rangle\langle i_r|H(\mathrm{EL})|i_{l'}\rangle}{E_a - E_r} . \qquad (28)$$

As the notation implies, the $\langle i_l|a\rangle$ are the expansion coefficients of a state $|a\rangle$ in terms of the eigenstate $|i_l\rangle$ in the limited space. If $k=1$, Eq. (27) represents the usual second-order nuclear polarization energy shifts. The inclusion of states with $k>1$ yields the nuclear polarization corrections to the hyperfine structure and effectively gives rise to small corrections (typically a few percent) to the nuclear multipole moments $\langle\gamma_2 I_2||\overline{M}^{2p_{1/2},2p_{3/2}}(E2)||\gamma_1 I_1\rangle$.

In the present work, nuclear polarization corrections were calculated using the methods of Ref. 31. A computer program RURP [32] written by Rinker was used to compute the energy shifts of the states of muonic ^{150,152}Sm using the known energies and EL transition matrix elements of the lower ex-

TABLE V. Corrections to muon binding energies (keV) for ^{150}Sm. The parameters listed in Table II were used to calculate the corrections. The magnitude of the $\alpha^2(Z\alpha)$ Lamb shifts can be used as an overall estimate of the magnitude of the error for the total correction except for the nuclear polarization correction.

State	Binding energy without correction	Vacuum polarization $\alpha(Z\alpha)$	Vacuum polarization $\alpha^2(Z\alpha)$	Vacuum polarization $\alpha(Z\alpha)^{n\geq 3}$	Muon	Lamb shift $\alpha(Z\alpha)$	Lamb shift $\alpha^2(Z\alpha)$	Relativistic recoil correction	Electron screening	Nuclear polarization	Dynamic $E2$ effect	Binding energy with correction
$1s_{1/2}$	7136.490	47.785	0.393	−0.206	0.173	−2.311	−0.113	0.286	0.001	4.340	...	7186.837
$2s_{1/2}$	2225.438	11.653	0.090	−0.087	0.028	−0.457	−0.019	0.052	0.008	0.594	...	2237.301
$2p_{1/2}$	2774.786	17.558	0.134	−0.123	0.015	−0.086	−0.028	0.048	0.004	1.052	2.123	2795.486
$2p_{3/2}$	2687.320	16.198	0.122	−0.118	0.010	−0.237	−0.024	0.041	0.004	0.937	3.196	2707.447
$3p_{3/2}$	1204.043	5.313	0.039	−0.051	0.004	−0.081	−0.009	0.011	0.020	0.175	0.165	1209.629
$3d_{3/2}$	1221.351	4.882	0.035	−0.058	0.000	+0.018	−0.002	0.006	0.014	0.030	0.020	1226.297
$3d_{5/2}$	1207.420	4.686	0.033	−0.055	0.000	−0.014	−0.001	0.006	0.015	0.023	0.018	1212.130
$4f_{5/2}$	680.475	1.685	0.012	−0.027	0.000	+0.004	−0.000	0.002	0.037	...	...	682.187
$4f_{7/2}$	677.547	1.656	0.011	−0.027	0.000	−0.003	−0.000	0.002	0.037	...	...	679.224

TABLE VI. Corrections to muon binding energies (keV) for ^{152}Sm. The parameters listed in Table III were used to calculate the corrections.

State	Binding energy without correction	Vacuum polarization $\alpha(Z\alpha)$	Vacuum polarization $\alpha^2(Z\alpha)$	Vacuum polarization $\alpha(Z\alpha)^{n\geq 3}$	Muon	Lamb shift $\alpha(Z\alpha)$	Lamb shift $\alpha^2(Z\alpha)$	Relativistic recoil correction	Electron screening	Nuclear polarization	Dynamic $E2$ effect	Binding energy with correction
$1s_{1/2}$	7110.194	47.460	0.389	−0.206	0.170	−2.283	−0.111	0.279	0.001	6.340	...	7162.234
$2s_{1/2}$	2221.057	11.603	0.090	−0.087	0.028	−0.452	−0.018	0.051	0.008	0.820	...	2233.100
$2p_{1/2}$	2772.769	17.515	0.134	−0.123	0.015	−0.086	−0.027	0.048	0.004	1.835	10.000	2802.084
$2p_{3/2}$	2685.966	16.170	0.122	−0.118	0.010	−0.237	−0.023	0.041	0.004	1.657	30.077	2733.670
$3p_{3/2}$	1203.576	5.304	0.040	−0.051	0.004	−0.081	−0.008	0.010	0.020	0.323	1.319	1210.455
$3d_{3/2}$	1221.346	4.883	0.035	−0.058	0.000	+0.018	−0.002	0.006	0.014	0.053	0.124	1226.419
$3d_{5/2}$	1207.424	4.686	0.033	−0.055	0.000	−0.015	−0.001	0.006	0.015	0.040	0.113	1212.245
$4f_{5/2}$	680.482	1.684	0.012	−0.027	0.000	+0.004	−0.000	0.002	0.037	...	...	682.194
$4f_{7/2}$	677.554	1.655	0.012	−0.027	0.000	−0.003	−0.000	0.002	0.037	...	...	679.231

cited states (see Table VII). The contributions of the higher excited states were approximated by concentrating all of the remaining EL strength into a single representative resonance state, whose energy was estimated by using an empirical expression for the EL giant resonance energy and whose strength was determined by using sum rules (corrected by subtraction of the transition strength of the lower excited states). The calculated nuclear polarization corrections are shown in Tables VIII and IX. The correction to the hyperfine structure expressed by the matrices $E^{(2)}_{l,l'}$ are given in footnotes to these tables.

In order to investigate the accuracy of the present second-order perturbation calculation, we have compared it with an exact calculation using the coupled-channel method of McKinley.[33] This exact calculation, which included only the nuclear ground and first excited 2^+ states, was made using a computer code written by Wills. The difference between the coupled-channel calculation and the perturbation method was less than 3% of the total nuclear polarization effect.

The uncertainty in the contribution of the lower excited states to the nuclear polarization is much smaller than our experimental uncertainties in determining the muonic binding energies since the nuclear properties of the low-lying states are reasonably well known. However, it is difficult to assess the uncertainty in the nuclear polarization arising from the giant resonance approximation used for the higher excited states. For convenience in estimating the influence of the nuclear polarization correction on our final results, derivatives of the quoted nuclear charge distribution parameters with respect to the $1s$ and $2p_{1/2}$ nuclear polarization corrections are listed in Table X.

3. *Isomer shift and magnetic hyperfine corrections for the 2p states*

The isomer shift and the magnetic hyperfine splitting of the $2^+ \otimes 1s_{1/2}$ state can be determined from the experimental data as will be discussed in Sec. IV A. The influence of these two effects on the $2^+ \otimes 2p$ states, however, is too small to be experimentally determined. Nevertheless, in order to extract accurate charge distribution and quadrupole moment parameters the energies of the $2^+ \otimes 2p$ states must be corrected for these effects.

The isomer shift of the $2^+ \otimes 2p$ states was estimated by assuming that the isomer shift in the effective Barrett radii R_k is the same for both the $2^+ \otimes 1s_{1/2}$ and the $2^+ \otimes 2p$ states. The energy splittings caused by the magnetic hyperfine interaction were computed by using the phonon model of Johnson and Sorensen.[34] This model,

TABLE VII. Properties of the lower excited states of ^{150}Sm and ^{152}Sm used in the analysis.

	^{150}Sm [a]			^{152}Sm		
State	Excitation energy (keV)	$\langle I^+\|\|M(E\lambda)\|\|0^+_g\rangle$ (e fm$^\lambda$)	$\langle I^+\|\|M(E\lambda)\|\|2^+_g\rangle$ (e fm$^\lambda$)	Excitation energy (keV)	$\langle I^+\|\|M(E\lambda)\|\|0^+_g\rangle$ (e fm$^\lambda$)	$\langle I^+\|\|M(E\lambda)\|\|2^+_g\rangle$ (e fm$^\lambda$)
2^+_g	333.95	115.3 ± 0.9 [b]	−169 ± 15	121.77	183.0 ± 2.0 [b,d]	−216 ± 21 [b,e]
4^+_g	773.35		211 ± 8	366.5		298 ± 5 [d]
0^+_β	740.4	9.7 ± 0.7 [c]	50 ± 3	684.8	9.7 ± 0.7 [f]	42 ± 2 [g]
2^+_β	1046.14	13.8 ± 1.1	−140 ± 22	810.4	15.1 ± 0.6 [g]	−36 ± 2 [g]
2^+_γ	1193.81	22.6 ± 1.1	46 ± 14	1085.79	28.5 ± 1.0 [g]	46 ± 2 [g]
3^-_1	1071.4	557 ± 18		1041	346 ± 43 [h]	
3^-_2				1058	265 ± 38 [h]	

[a] Reference 2.
[b] Used only for nuclear polarization calculation.
[c] Assumed to be the same as ^{152}Sm.
[d] Reference 5.
[e] Weighted average of Refs. 6 and 7.
[f] Reference 8.
[g] Reference 9.
[h] Reference 10.

which assumes a surface current of angular momentum I at a radius R_0, yields a magnetic hyperfine constant A given by

$$A=\frac{2e\kappa}{j+1}g_R\mu_N I\left[\int_{R_0}^{\infty}f_{n\kappa}(r)g_{n\kappa}(r)dr+\frac{1}{R_0^3}\int_0^{R_0}f_{n\kappa}(r)g_{n\kappa}(r)r^3dr\right]. \quad (29)$$

With $R_0=6.5$ fm and the experimental gyromagnetic ratio[20] $g_R=0.35$ for ^{152}Sm, the magnetic interaction energies for $2^+\otimes 2p_{1/2}$ ($F=\frac{3}{2}$), $2^+\otimes 2p_{3/2}$ ($F=\frac{1}{2}$), and $2^+\otimes 2p_{3/2}$ ($F=\frac{3}{2}$) have the values of -0.136, -0.115, and -0.076 keV, respectively. The total effect of the magnetic corrections is to reduce the quadrupole moment $\langle 2^+\|\overline{M}^{2p_{1/2},2p_{3/2}}(E2)\|2^+\rangle$ by about 0.6%.

IV. RESULTS OF ANALYSIS

The following analysis of the muonic atom data of ^{150}Sm and ^{152}Sm is separated into two principal parts. In subsection B the muonic data are analyzed using a specific nuclear charge distribution. This analysis follows the traditional approach to muonic atom data, and yields values for the model parameters and the electromagnetic moments of the lower nuclear excited states. In subsection C the analysis is extended by employing the theoretical methods of Sec. III which allow one to extract certain model-independent parameters. In order to use either analysis method, several peripheral but essential matters must be considered first. These are discussed in subsection A.

A. Isomer shifts and magnetic hyperfine splittings

If the energies of the K x rays are precisely determined, they can be used to determine the isomer shift and magnetic hyperfine splitting of the $2^+\otimes 1s_{1/2}$ states. For example, the difference in the energy of the two K x rays that are emitted from the same $2p$ hyperfine component reflects the energy difference between the $2^+\otimes 1s_{1/2}$ and $0^+\otimes 1s_{1/2}$ states as shown in Fig. 5 for ^{152}Sm. The isomer shift value of 1.00 ± 0.20 keV for ^{152}Sm extracted in this way is in good agreement with the values of 0.85 ± 0.07 and 0.91 ± 0.08 that were obtained previously from the $2^+\to 0^+\gamma$ rays.[20,35] Although the previous values have smaller quoted errors than the present value, it should be kept in mind that they involve a theoretical correction for the interdoublet $M1$ transition. The present determination is based directly on the measured energy difference and is free from possible theoretical ambiguities. Agreement between the present and the previous values indicates that the theoretical estimate of the $M1$ effect is correct within the accuracy obtained here.

The 2^+ state in ^{150}Sm was not excited strongly enough to permit the isomer shift to be determined by the K x rays. Instead, the determination has been made in the usual way from the observed nuclear γ-ray energy. The correction for the $M1$ interdoublet transition was calculated as described in Refs. 20 and 35. In ^{150}Sm this correction is small (30 eV) compared to the experimental error involved in the determination of the γ-ray energy, since the relatively high energy of the 2^+ state of ^{150}Sm results in an $E2$ transition rate which is much faster than the $M1$ transition rate.

The magnetic hyperfine splitting can, in principle, also be determined since the K transition $0^+\otimes 2p_{1/2}\to 2^+\otimes 1s_{1/2}$ populates only the $F=\frac{3}{2}$ component of the $2^+\otimes 1s_{1/2}$ state, while 99% and 90% of the K x rays $0^+\otimes 2p_{3/2}\to 2^+\otimes 1s_{1/2}$ and $2^+\otimes 2p_{1/2}$

TABLE VIII. Nuclear polarization corrections to muon binding energies (keV) for ^{150}Sm. States I_s^π and I_v^π are isoscalar and isovector resonance states, respectively. States I_n^π ($n = g,\beta,\gamma$) are lower excited states whose properties are given in Table VII. Nuclear polarization subtotals for the high- and low-lying states are represented by ΔB_{NP}^H and ΔB_{NP}^L, respectively. Effects of $E2$ excitations on $2p$ and $3d$ states are expressed in matrix form $\Delta E_{ll'}^{(2)}$ and given in footnotes a–d.

Nuclear state	$1s_{1/2}$	$2s_{1/2}$	$2p_{1/2}$	$2p_{3/2}$	$3p_{3/2}$	$3d_{3/2}$	$3d_{5/2}$
0_s^+	0.548	0.129	0.016	0.008	0.003	0.000	0.000
0_v^+	0.235	0.049	0.008	0.004	0.001	0.000	0.000
1_v^-	1.157	0.163	0.296	0.264	0.085	0.014	0.012
2_s^+	0.293	0.032	0.088	0.079	0.025	0.004	0.003
2_v^+	0.144	0.016	0.035	0.031	0.010	0.001	0.001
$3_s^-, 3_v^-$	0.120	0.013	0.027	0.023	0.008	0.001	0.000
$4_s^+, 4_v^+$	0.120	0.013	0.026	0.022	0.007	0.001	0.000
$5_s^-, 5_v^-$	0.056	0.006	0.011	0.009	0.003	0.000	0.000
ΔB_{NP}^H	2.673	0.421	0.507	0.440	0.142	0.021	0.016
0_β^+	0.152	0.005	0.001	0.001	0.000	0.000	0.000
2_g^+	1.328	0.148	a	b	0.035	c	d
2_β^+	0.018	0.002	a	b	−0.002	c	d
2_γ^+	0.049	0.005	a	b	−0.012	c	d
3_1^-	0.120	0.013	0.038	0.034	0.012	−0.003	−0.003
ΔB_{NP}^L	1.667	0.173	0.039	0.035	0.033	−0.003	−0.003
Total ΔB_{NP}	4.340	0.594	0.546	0.475	0.175	0.018	0.013

[a] $F=\frac{1}{2}^-$:

$$\begin{array}{l} 2p_{1/2} \\ 2_g^+\otimes 2p_{3/2} \end{array}\begin{bmatrix} -0.506 & \\ +0.359 & -1.078 \end{bmatrix}.$$

[b] $F=\frac{3}{2}^-$:

$$\begin{array}{l} 2p_{3/2} \\ 2_g^+\otimes 2p_{1/2} \\ 2_g^+\otimes 2p_{3/2} \end{array}\begin{bmatrix} -0.462 & & \\ -0.246 & -0.901 & \\ +0.239 & +0.242 & -0.834 \end{bmatrix}.$$

[c] $F=\frac{3}{2}^+$:

$$\begin{array}{l} 3d_{3/2} \\ 2_g^+\otimes 3d_{3/2} \\ 2_g^+\otimes 3d_{5/2} \end{array}\begin{bmatrix} -0.012 & & \\ -0.006 & -0.013 & \\ -0.005 & +0.004 & -0.013 \end{bmatrix}.$$

[d] $F=\frac{5}{2}^+$:

$$\begin{array}{l} 3d_{5/2} \\ 2_g^+\otimes 3d_{3/2} \\ 2_g^+\otimes 3d_{5/2} \end{array}\begin{bmatrix} -0.009 & & \\ +0.004 & -0.027 & \\ -0.007 & -0.008 & -0.010 \end{bmatrix}.$$

The space diagonalized ("limited space") consists of the 0_g^+, 2_g^+, 4_g^+, 0_β^+, 2_β^+, and 2_γ^+ states.

$\rightarrow 2^+\otimes 1s_{1/2}$, respectively, populate the $F=\frac{5}{2}$ component. In contrast to the isomer shift, the magnetic splitting could only be determined with a relatively large error, and then only for ^{152}Sm, because of the low intensity of the $0^+\otimes 2p_{1/2} \rightarrow 2^+\otimes 1s_{1/2}$ transition. The values obtained for the isomer shifts and magnetic hyperfine splitting are listed in Table X.

B. Fitted parameters

In the analysis of ^{152}Sm the K and L transition energies were used to determine the six parameters c, a, $\langle 2^+||M(E2)||0^+\rangle$, $\langle 2^+||M(E2)||2^+\rangle$, the isomer shift and magnetic hyperfine splitting of the $2^+\otimes 1s_{1/2}$ state, simultaneously. Other matrix elements used in the analysis were held constant

TABLE IX. Nuclear polarization corrections to muon binding energies (keV) for ^{152}Sm. See Table VIII for notation.

Nuclear state	$1s_{1/2}$	$2s_{1/2}$	$2p_{1/2}$	$2p_{3/2}$	$3p_{3/2}$	$3d_{3/2}$	$3d_{5/2}$
0_s^+	0.540	0.128	0.015	0.008	0.003	0.000	0.000
0_v^+	0.237	0.049	0.008	0.004	0.001	0.000	0.000
1_v^-	1.163	0.164	0.300	0.267	0.086	0.014	0.012
2_s^+	0.288	0.032	0.087	0.078	0.025	0.004	0.003
2_v^+	0.145	0.016	0.036	0.031	0.010	0.001	0.000
$3_s^-, 3_v^-$	0.118	0.013	0.027	0.023	0.008	0.000	0.000
$4_s^+, 4_v^+$	0.120	0.013	0.026	0.022	0.007	0.000	0.000
$5_s^-, 5_v^-$	0.056	0.006	0.011	0.009	0.003	0.000	0.000
$\Delta B_{\rm NP}^H$	2.667	0.421	0.510	0.442	0.143	0.019	0.015
0_β^+	0.160	0.005	0.001	0.001	0.000	0.000	0.000
2_g^+	3.338	0.375	a	b	0.184	c	d
2_β^+	0.022	0.002	a	b	0.000	c	d
2_γ^+	0.080	0.009	a	b	−0.011	c	d
3_1^-	0.046	0.005	0.014	0.013	0.004	−0.001	−0.001
3_2^-	0.027	0.003	0.008	0.008	0.003	−0.001	−0.001
$\Delta B_{\rm NP}^L$	3.673	0.399	0.023	0.022	0.180	−0.002	−0.002
Total $\Delta B_{\rm NP}$	6.340	0.820	0.533	0.464	0.323	0.017	0.013

[a] $F=\frac{1}{2}^-$:

$$\begin{array}{l} 2p_{1/2} \\ 2_g^+ \otimes 2p_{3/2} \end{array} \begin{bmatrix} -1.302 & \\ +0.687 & -1.777 \end{bmatrix}.$$

[b] $F=\frac{3}{2}^-$:

$$\begin{array}{l} 2p_{3/2} \\ 2_g^+ \otimes 2p_{1/2} \\ 2_g^+ \otimes 2p_{3/2} \end{array} \begin{bmatrix} -1.193 & & \\ -0.470 & -1.374 & \\ +0.457 & +0.540 & -1.272 \end{bmatrix}.$$

[c] $F=\frac{3}{2}^+$:

$$\begin{array}{l} 3d_{3/2} \\ 2_g^+ \otimes 3d_{3/2} \\ 2_g^+ \otimes 3d_{5/2} \end{array} \begin{bmatrix} -0.036 & & \\ -0.008 & -0.037 & \\ -0.008 & -0.004 & -0.027 \end{bmatrix}.$$

[d] $F=\frac{5}{2}^+$:

$$\begin{array}{l} 3d_{5/2} \\ 2_g^+ \otimes 3d_{3/2} \\ 2_g^+ \otimes 3d_{5/2} \end{array} \begin{bmatrix} -0.027 & & \\ +0.006 & -0.045 & \\ -0.012 & -0.003 & -0.033 \end{bmatrix}.$$

at the values listed in Table VII. The parameters β_2 and β_4 of the deformed Fermi distribution used in the analysis [Eqs. (22) and (25)] were held fixed at values listed in Table X. Calculated values were used for the nuclear polarization corrections and the isomer shifts and magnetic hyperfine shifts of the $2^+ \otimes 2p$ states, as discussed in the previous section.

The muonic x-ray spectrum of ^{150}Sm displayed only the usual K x-ray doublet characteristic of a "spherical" nucleus because the excitation energy of the lowest 2^+ state in ^{150}Sm is much larger than the $2p$ fine-structure splitting. Therefore, in the analysis of the ^{150}Sm data, the values of only the three parameters c, a, and $\langle 2^+ || M(E2) || 0^+ \rangle$ were determined from the K and L transition energies.

The values of the fitted parameters for both ^{150}Sm and ^{152}Sm are listed in Table X. The errors in the fitted quantities were derived using the following procedure. A first simultaneous fit of the above six parameters for ^{152}Sm and for the three parameters of ^{150}Sm was made using only the statistical errors arising in the measurements of the transition energies, to determine the central values and correlated statistical errors of the fitted parame-

TABLE X. Results of the analysis performed using a deformed Fermi charge distribution. The errors include uncertainties in radiative corrections and spectroscopic parameters in addition to experimental errors. To indicate the sensitivity of our measurements to the nuclear polarization corrections, we have listed the derivatives of the parameters with respect to the nuclear polarization corrections of the $1s_{1/2}$ and $2p_{1/2}$ states holding the ratio of $\Delta B^H_{NP}(2p_{3/2})/\Delta B^H_{NP}(2p_{1/2})$ fixed. The units of the derivatives are (units of the parameter)/keV.

	^{150}Sm			^{152}Sm		
	Zero β_4	Derivative with respect to $\Delta B^H_{NP}(1s_{1/2})$ (keV^{-1})	Derivative with respect to $\Delta B^H_{NP}(2p_{1/2})$ (keV^{-1})	Nonzero β_4	Zero β_4	Derivative with respect to $\Delta B^H_{NP}(1s_{1/2})$ (keV^{-1})	Derivative with respect to $\Delta B^H_{NP}(2p_{1/2})$ (keV^{-1})
c (fm)	5.856 ±0.030	+0.015	−0.237	5.885 ±0.012	5.871 ±0.012	+0.013	−0.156
a (fm)	0.557 ±0.016	−0.007	+0.125	0.545 ±0.007	0.554 ±0.007	−0.006	+0.085
β_2	0.231 (fixed)			0.284 (fixed)	0.297 (fixed)		
β_4	0.0 (fixed)			0.070 (fixed)	0.000 (fixed)		
$\langle r^2\rangle^{1/2}$ (fm)	5.0470 ±0.0024	+0.0004	+0.0218	5.0938 ±0.0011	5.0938 ±0.0011	+0.0006	+0.0143
$\langle 2^+ \Vert M(E2) \Vert 0^+\rangle$ (e fm^2)	121.4 ±3.7	−0.6	+17	185.94 ±0.24	183.55 ±0.24	−0.008	+0.016
$\langle 2^+ \Vert M(E2) \Vert 2^+\rangle$ (e fm^2)	−169 (fixed)			−224.6 ±2.2	−221.7 ±2.2	+0.3	−0.7
$R(22, 02)$				1.010 ±0.012	1.010 ±0.012	−0.001	+0.003
HF splitting of $2^+ \otimes 1s_{1/2}$ (keV)[a]				0.70 ±0.47			
Isomer shift of $2^+ \otimes 1s_{1/2}$ (keV)[a]	2.72 ±0.14[b]			1.00 ±0.20			
Isomer shift $\delta\langle r^2\rangle$ (fm^2)	0.0496 ±0.0026			0.018 ±0.004			

[a] Independent of the charge distribution model.

[b] Obtained from the measured γ-ray energy.

ters. The errors in the parameters resulting from the (systematic) energy calibration error were estimated by a second fit of the data using transition energies shifted by an amount equal to the calibration errors. The difference between the central values of the two fits was added quadratically to the correlated statistical error of each parameter. The effect of the uncertainties in the fixed matrix elements (Table VII) was found to be negligibly small compared to the statistical and calibration errors. We have included no contribution for the uncertainties of the nuclear polarization calculation in the quoted errors. However, to indicate the sensitivity of our measurements to the nuclear polarization corrections, we have listed in Table X the derivatives of the parameters with respect to the nuclear polarization corrections of the $1s$ and $2p_{1/2}$ states.

Tables II and III present a comparison of the observed and calculated transition energies and intensities for ^{150}Sm and ^{152}Sm. The intensity agreement between theory and experiment was satisfactory (cf. the χ^2 values listed in Tables II and III), except for the $3p_{3/2} \rightarrow 2s_{1/2}$ and $2s_{1/2} \rightarrow 2p_{3/2}$ transitions. The populations of the initial states of these transitions were not well estimated by the cascade program used in the intensity calculation since this program considered only the lowest multipole-order ($E1$) x-ray transitions.

It has been pointed out by Chen[36] that $E1$ transition matrix elements are affected by nuclear polarization effects. Although inclusion of these effects in the present calculation resulted in slightly improved agreement with the observed intensities, the effect was small compared to the experimental errors.

In both ^{150}Sm and ^{152}Sm, the energies of transitions involving the $2s_{1/2}$ state are not in agreement with theoretical predictions. However, if the nuclear polarization corrections of the $2s_{1/2}$ state are decreased by about 650 eV in ^{150}Sm and 300 eV in ^{152}Sm, satisfactory agreement is obtained. The tendency of the "theoretical" $2s_{1/2}$ nuclear polarization correction to appear to be too large when $2s_{1/2}$ muonic x rays are analyzed on the basis of a computed $1s_{1/2}$ nuclear polarization correction has been observed in other muonic atom measurements and will be the subject of a separate publication.[37]

C. Extraction of model-independent parameters

The model-dependent parameters determined above may be used to derive model-independent parameters by using the analysis theory discussed in Sec. III. In order to extract the equivalent Barrett radii R_k and the sensitivities $C_Z = dR_k/dE$, we determined the three parameters of the Barrett approximation for the muon-generated potential (A, B, and k) for the muonic transition energies by a fit to the exact potential calculated from the Dirac equation. Following the procedure used in Ref. 20, the value of α was held constant at 0.125. With these values, the Barrett radii of the fitted reference charge distribution $\rho^{\mathrm{DF}}(r)$ and sensitivities C_Z were computed. The results are shown in Table XI.

The isotope shifts δR_k of the equivalent Barrett radii of ^{150}Sm and ^{152}Sm were determined from the relation $\delta R_k = C_Z \delta E$, where δE is the difference of the transition energies of ^{150}Sm and ^{152}Sm (corrected for dynamic nuclear interactions). The isotope shift values are given in Table XII. Values of the model-independent generalized quadrupole moments $\langle \gamma_2 I_2 \| \bar{M}^{2p_{1/2},2p_{3/2}}(E2) \| \gamma_1 I_1 \rangle$ have been converted from the model-dependent fitted parameters $\langle \gamma_2 I_2 \| M(E2) \| \gamma_1 I_1 \rangle$ using Eqs. (14) and (25). The values of $\langle \gamma_2 I_2 \| \bar{M}^{2p_{1/2},2p_{3/2}}(E2) \| \gamma_1 I_1 \rangle$ for ^{150}Sm and ^{152}Sm and of the ratio $R(22,02)$ for ^{152}Sm are listed in Table XIII.

As an initial step in deriving quadrupole radii, values for the parameters A, B, and m of Eq. (13) were determined in a manner similar to that discussed above for the monopole radii by fitting the computed $2p_{1/2}$-$2p_{3/2}$ transition potential. Quadrupole radii R_m were then computed from Eq. (17) using these parameters and experimental values of the matrix elements $\langle \gamma_2 I_2 \| M(E2) \| \gamma_1 I_1 \rangle$ obtained from Coulomb excitation.[2,6,7,13] In addition the sensitivity C_R, the dependence of the ratio $R(22,02)$ on the difference δR_m of the two quadrupole radii R_m, was computed using Eqs. (19) and (20). Values of these quadrupole charge parameters are summarized in Table XIII.

V. DISCUSSION OF RESULTS AND CONCLUSIONS

A. Comparison with other experimental results

High precision measurements of the ^{150}Sm and ^{152}Sm muonic x-ray spectra together with refined methods of analysis have provided precise values for the charge parameters and electromagnetic moments of these nuclei. Nearly model-independent values of the monopole charge distribution (Barrett moments and equivalent radii R_k) have been obtained and the isotope shift for ^{152}Sm-^{150}Sm has been determined. The measured Sm isotope shift is about twice as large as the "standard" shift value $\delta R_{k,\mathrm{STD}} = \frac{1}{3}(\delta A/A)R_k = 0.028$ fm and is larger than the usual variation which is associated with changes in the neutron shell structure.[23] The unusually large shifts observed previously for ^{150}Nd-^{148}Nd and for ^{154}Gd-^{152}Gd (Ref. 38) and ob-

TABLE XI. Equivalent Barrett radii of ^{150}Sm and ^{152}Sm ($\alpha = 0.125$ fm^{-1}). Errors include both experimental errors and ambiguities in the dynamic $E2$ effect, but not ambiguities in nuclear polarization corrections. We note that all the R_k values are not entirely independent quantities since correlations involving the $2p$ states are introduced by the extraction of the dynamic $E2$ effect.

Isotope	Transition	k	B (keV/fm^4)	C_Z (fm/keV)	Exp. Energy	R_k(fm)
^{150}Sm	$2p_{3/2}$-$1s_{1/2}$	2.2297	1.6239	-2.185×10^{-3}	4479.41 ± 0.39	6.4374 ± 0.0009
	$2p_{1/2}$-$1s_{1/2}$	2.2206	1.6139	-2.245×10^{-3}	4391.33 ± 0.33	6.4364 ± 0.0008
	$3d_{3/2}$-$2p_{1/2}$	3.5482	6.8255×10^{-3}	-3.038×10^{-2}	1569.09 ± 0.24	6.5709 ± 0.0073
	$3d_{5/2}$-$2p_{3/2}$	4.0253	1.6381×10^{-3}	-4.713×10^{-2}	1495.32 ± 0.30	6.613 ± 0.014
	$3d_{3/2}$-$2p_{3/2}$	4.0229	1.6374×10^{-3}	-4.739×10^{-2}	1481.23 ± 0.31	6.607 ± 0.015
	$3p_{3/2}$-$2s_{1/2}$	1.8838	5.9315×10^{-1}	-1.342×10^{-2}	1026.98 ± 0.15	6.4076 ± 0.0020
	$2s_{1/2}$-$2p_{3/2}$	1.5118	−1.2200	$+1.672\times10^{-2}$	470.75 ± 0.30	6.3575 ± 0.0050
	$2^+\otimes 1s_{1/2}$-$1s_{1/2}$ [a]	2.3016	−1.4496	$+2.080\times10^{-3}$	2.72 ± 0.14	0.0057 ± 0.0003
^{152}Sm	$2p_{3/2}$-$1s_{1/2}$	2.2335	1.5956	-2.202×10^{-3}	4428.56 ± 0.33	6.4927 ± 0.0007
	$2p_{1/2}$-$1s_{1/2}$	2.2245	1.5857	-2.261×10^{-3}	4360.12 ± 0.28	6.4918 ± 0.0006
	$3d_{3/2}$-$2p_{1/2}$	3.5534	6.6956×10^{-3}	-3.017×10^{-2}	1575.60 ± 0.14	6.6334 ± 0.0042
	$3d_{5/2}$-$2p_{3/2}$	4.0303	1.6100×10^{-3}	-4.649×10^{-2}	1521.40 ± 0.24	6.680 ± 0.011
	$3d_{3/2}$-$2p_{3/2}$	4.0279	1.6092×10^{-3}	-4.675×10^{-2}	1507.41 ± 0.27	6.671 ± 0.013
	$3p_{3/2}$-$2s_{1/2}$	1.8889	5.8357×10^{-1}	-1.350×10^{-2}	1022.30 ± 0.25	6.4560 ± 0.0034
	$2s_{1/2}$-$2p_{3/2}$	1.5173	−1.1982	$+1.688\times10^{-2}$	500.83 ± 0.28	6.4035 ± 0.0047
	$2^+\otimes 1s_{1/2}$-$1s_{1/2}$ [a]	2.3060	−1.4228	$+2.094\times10^{-3}$	0.99 ± 0.20	0.0021 ± 0.0004

[a] Isomer shift.

served here for ^{152}Sm-^{150}Sm suggest a sudden change in shape between these pairs of nuclei. Such a sudden change in shape is also consistent with the observation that the lighter nucleus of each pair has a low-lying spectrum typical of spherical nuclei, while the heavier nucleus has a spectrum typical of deformed nuclei.

In order to test the consistency of the present muonic isotope shift δR_k with previous optical or electronic x-ray isotope shift measurements, we have estimated the mean-square-radius isotope shift using two methods. First, assuming that the ratio $\langle r^2\rangle^{1/2}/R_k$ is the same for both ^{150}Sm and ^{152}Sm, we obtained the values listed in the last column of Table XII, in fair agreement with the previous measurements.[38] (The value of the ratio $\langle r^2\rangle^{1/2}/R_k$ was calculated from the values for ^{150}Sm.) It is also possible to estimate $\delta\langle r^2\rangle$ directly from the parameters fitted to the deformed Fermi distribution (see Table X). Using this method, we obtained $\delta\langle r^2\rangle = 0.475(58)$ fm^2, which is consistent with the previous results. However, the uncertainties arising from the strong correlation between the charge model parameters and from the model dependence of the Fermi distribution tend to make this method of determining $\delta\langle r^2\rangle$ isotope shifts unreliable.

The generalized muonic static and transition quadrupole moments of the 2_g^+ state of ^{152}Sm and the generalized muonic transition quadrupole moment of the 2_g^+ state of ^{150}Sm have been determined. From these generalized moments the quadrupole moment $Q(2^+)$ of ^{152}Sm and the $B(E2; 0^+ \to 2^+)$ values of ^{150,152}Sm were obtained by introducing a specific form $F_2(r)$ for the transition charge density. The results are compared in Table XIV with previous

TABLE XII. Isotope shifts of the ^{150,152}Sm isotopes ($\alpha = 0.125$ fm^{-1}). The value for ^{152}Sm minus the value for ^{150}Sm is given for the energy difference, δR_k and $\delta\langle r^2\rangle$. See text for derivations of $\delta\langle r^2\rangle$.

Transition	k	C_Z (fm/keV)	Energy difference (keV)	δR_k (fm)	$\delta\langle r^2\rangle$ (fm^2)
$2p_{3/2}$-$1s_{1/2}$	2.2297	-2.185×10^{-3}	−25.25 ± 0.35	0.0552 ± 0.0008	0.437 ± 0.006
$2p_{1/2}$-$1s_{1/2}$	2.2206	-2.245×10^{-3}	−24.57 ± 0.22	0.0552 ± 0.0005	0.437 ± 0.004
$3d_{3/2}$-$2p_{1/2}$	3.5482	-3.038×10^{-2}	−2.01 ± 0.26	0.0665 ± 0.0079	0.516 ± 0.061
$3d_{5/2}$-$2p_{3/2}$	4.0253	-4.713×10^{-2}	−1.39 ± 0.37	0.0655 ± 0.0175	0.505 ± 0.135
$3d_{3/2}$-$2p_{3/2}$	4.0229	-4.739×10^{-2}	−1.28 ± 0.40	0.0607 ± 0.0190	0.468 ± 0.146
$3p_{3/2}$-$2s_{1/2}$	1.8838	-1.342×10^{-2}	−3.60 ± 0.26	0.0483 ± 0.0035	0.383 ± 0.028
$2s_{1/2}$-$2p_{3/2}$	1.5118	$+1.672\times10^{-2}$	+2.72 ± 0.40	0.0455 ± 0.0068	0.365 ± 0.054

TABLE XIII. Generalized quadrupole moments and equivalent quadrupole radii of the Sm isotopes (model-independent analysis). The values of m, A, and B were obtained by using muon wave functions calculated with the parameters given in Tables II and III. The sensitivity of R_m to change in the generalized moment are given by

$$C_m = \langle I_2 \| M(E2) \| I_1 \rangle \frac{\partial R_m}{\partial \langle I_2 \| \overline{M}^{2p_{1/2},2p_{3/2}}(E2) \| I_1 \rangle} .$$

See Eqs. (17)–(20) for other notations.

Isotope	^{150}Sm	^{152}Sm
α (fm^{-1})	0.125	0.125
m	2.258 7	2.262 7
A	1.003 5	0.998 6
B(fm^{-m})	−0.010 712	−0.010 534
R_m^{DEF} (fm)	6.646	6.837
$\langle 2^+ \| \overline{M}^{2p_{1/2},2p_{3/2}}(E2) \| 0^+ \rangle$ (e fm^2)	81.0 ± 3.6	121.14 ± 0.16
$\langle 2^+ \| M(E2) \| 0^+ \rangle$ (e fm^2)	114.9 ± 0.9 [a]	185.01 ± 0.41 [b]
R_m^{02} (fm)	6.12 ± 0.43	6.791 ± 0.024
C_m^{02} (fm)	−13.735	−13.970
$\langle 2^+ \| \overline{M}^{2p_{1/2},2p_{3/2}}(E2) \| 2^+ \rangle$ (e fm^2)		−146.3 ± 1.5
$\langle 2^+ \| M(E2) \| 2^+ \rangle$ (e fm^2)		−216 ± 21 [c]
R_m^{22} (fm)		6.49 ± 0.92
C_m^{22} (fm)		−13.878
R(22, 02)		1.010 ± 0.012
$\delta R_m = R_m^{22} - R_m^{02}$ (fm)		−0.05 ± 0.11 [d]
C_R (fm)		−9.147

[a] Reference 2. Obtained from Coulomb excitation.
[b] Reference 13.
[c] References 6 and 7.
[d] See Sec. V B.

results based on Coulomb excitation and radioactive decay data. Small differences between the "point-nucleus" moments derived from muonic x-ray data and those from Coulomb excitation should not necessarily be interpreted as a disagreement between the two experiments, since a specific form must be assumed for the transition charge density to reduce the measured muonic moments to "point-nucleus" values. For example, the extracted $B(E2; 0^+ \rightarrow 2^+)$ value of ^{152}Sm decreases by 2.5% if, instead of the experimental electron scattering values[12] of $\beta_2 = 0.284$ and $\beta_4 = 0.07$, the values $\beta_2 = 0.297$ and $\beta_4 = 0$, which are equally compatible with the observed muon energies, are used to define the charge distribution.

Equivalent quadrupole radii R_m were determined from the generalized muonic quadrupole moments by comparison with the point-nucleus moments. This extracted value of R_m contains all the information which is available from the present measurement concerning the form factor $F_2(r)$ of the transition charge density. Therefore, any form factor $F_2(r)$ of Sm which reproduces the value of R_m will be entirely consistent with both the muonic and point-nucleus measurements.

The ratio R(22, 02) of the generalized static and transition quadrupole moments has been derived for ^{152}Sm. In contrast to ^{150}Sm, the ratio R(22, 02) for ^{152}Sm is in excellent agreement with the pure rotational value of unity. However, this agreement does not necessarily imply a pure rotational character for the 2^+ state in ^{152}Sm. In fact, the nonzero isomer shift of the 2^+ state indicates a departure from the rotational model. The implications of these results will be explored in the following section.

B. Comparison with theory

Mixing of the β and γ bands may be important in understanding the ground-state band in ^{152}Sm. The Hamiltonian which couples the rotation and intrinsic motion may be written as[26]

$$H_c = \tfrac{1}{2}h_0(I_+I_- + I_-I_+) + \tfrac{1}{2}h_2(I_+^2 + I_-^2), \qquad (30)$$

where h_0 and h_2 are operators that cause $\Delta K = 0$ and $\Delta K = \pm 2$ mixing, respectively. If we assume that h_0 and h_2 are independent of spin I, first-or-

TABLE XIV. Comparison of the present experimental results with those of other experiments and with theoretical values.

	Experiment					Theory				
	μ x ray (Present)	μ x ray (Previous)	Optical and electronic x ray	Coulomb excitation	Lifetime	Kumar [j]	Kishimoto-Tamura [k]	Meyer-Speth [l]	Negle-Rinker [m]	Flocard *et al.* [n]
^{150}Sm										
$B(E2; 0^+ \rightarrow 2^+)(e^2b^2)$	1.47 ±0.09			1.32 ±0.02 [e]	1.36 ±0.05 [i]	1.16	1.35			
$Q(2^+)$(e b)				−1.28 ±0.11 [e]		−0.95	−1.17			
$R(22, 02)$				1.23 ±0.11 [f]		0.97	1.11			
$\langle r^2\rangle^{1/2}$ (fm)	5.0470 ±0.0024									
$\delta\langle r^2\rangle_{\text{isom}}$ (fm^2)	0.0496 ±0.0026					0.056				
^{152}Sm										
$B(E2; 0^+ \rightarrow 2^+)(e^2b^2)$	3.457 ±0.009	3.40 ±0.12 [b]		3.423 ±0.015 [g]	3.350 ±0.075 [i]	3.25	3.49		1.70	3.39
$Q(2^+)$(e b)	−1.702 ±0.017			−1.64 ±0.16 [h]		−1.64	−1.72			
$R(22, 02)$	1.010 ±0.012			0.98 ±0.16 [f]		1.00	1.02			
$\langle r^2\rangle^{1/2}$ (fm)	5.0938 ±0.0011	5.090 [b]							5.053	5.160
$\delta\langle r^2\rangle_{\text{isom}}$ (fm^2)	0.018 ±0.004	0.014 [c]				0.044		0.015		
Isotope shift										
$\delta\langle r^2\rangle_{\text{isot}}$ (fm^2)	0.437 ±0.004 [a]		0.424 ±0.011 [d]							

[a] Estimated from $2p_{1/2}$-$1s_{1/2}$ transition energies. See Table XII.
[b] Reference 11.
[c] References 20 and 35.
[d] Reference 38.
[e] Reference 2.
[f] $\delta R_m = 0$ assumed.
[g] Reference 13.
[h] References 6 and 7.
[i] Reference 5.
[j] Time-dependent Hartree-Bogoliubov treatment of the PPQ model: Ref. 15.
[k] Boson expansion treatment of the PPQ model: Ref. 16.
[l] Cranking model with Coriolis antipairing: Ref. 41.
[m] Density-dependent Hartree-Fock calculation: Ref. 42.
[n] Hartree-Fock calculation of Skyrme's interaction: Ref. 43.

der perturbation theory predicts that the $E2$ transition matrix element is a simple function of the spins of the states involved in the transitions.[26] The rotation-vibration-interaction (RVI) formalism can be used to extract mixing parameters z_γ and z_β from the γ to ground band transitions and from the β to ground band transitions, respectively. As shown by Riedinger *et al.*[8] and by Fraser *et al.*,[9] the RVI phenomenological model reproduces the transition probabilities between ground and γ bands of ^{152}Sm well with $z_\gamma = 0.09$.[8,9] Although $z_\beta = 0.08$ satisfactorily reproduces the transition probabilities for the $0_g^+ \to 2_\beta^+$, $2_g^+ \to 2_\beta^+$, and $2_g^+ \to 0_\beta^+$ transitions, no single z_β parameter can satisfactorily describe all the properties of mixing between the ground and β bands. However, an extension of the RVI treatment which takes into account the spin-dependence of h_0 can reproduce all of the observed ground-β $E2$ transition probabilities.[39] Using parameters $a(I) = \frac{1}{2}\langle n_\beta = 0 | h_0(I) | n_\beta = 1\rangle$, we can redefine the mixing parameter z_β:

$$z_\beta(I_\beta, I) = \bar{z}_\beta \alpha_-(I_\beta, I), \tag{31}$$

where

$$\alpha_\pm(I', I) = \frac{1}{I(I+1) \pm I'(I'+1)} \times \left[\frac{a(I)}{a(2)} I(I+1) \pm \frac{a(I')}{a(2)} I'(I'+1)\right]. \tag{32}$$

It is noted that $\alpha_\pm(2, 0) = \alpha_\pm(0, 2) = \alpha_\pm(2, 2) = 1$ and $\bar{z}_\beta = z_\beta(0, 2) = z_\beta(2, 0) = z_\beta(2, 2)$. With this definition, the value $\bar{z}_\beta = 0.08$ is consistent with all of the measured *interband* $E2$ transition probabilities.

Extending the modified RVI formalism to the intraband $E2$ matrix elements, we obtain

$$\langle I_g' \| M(E2) \| I_g \rangle = (2I_g' + 1)^{1/2} \langle I_g' 020 | I_g 0 \rangle Q_g \times \{1 + \zeta_\gamma \mathcal{F}_\gamma(I_g', I_g) + \zeta_\beta(I_g', I_g) \times [I_g(I_g+1) + I_g'(I_g'+1)]\}, \tag{33}$$

where

$$\mathcal{F}_\gamma(I', I) = \frac{f_\gamma(I)\langle I'022 | I2\rangle + f_\gamma(I')\langle I'22-2 | I0\rangle}{\sqrt{12}\,\langle I'020 | I0\rangle} \tag{34a}$$

and

$$f_\gamma(I) = [2I(I-1)(I+1)(I+2)]^{1/2}. \tag{34b}$$

The parameters ζ_γ and ζ_β are related to z_γ and to $\bar{z}_\beta$ by

$$\zeta_\gamma = \left(\frac{Q_\gamma}{Q_g}\right)^2 z_\gamma \tag{35}$$

and

$$\zeta_\beta(I', I) = \left(\frac{Q_\beta}{Q_g}\right)^2 \bar{z}_\beta \alpha_+(I', I), \tag{36}$$

where Q_g, Q_γ, and Q_β are intrinsic $E2$ matrix elements between the ground band and the ground, γ, and β bands, respectively, as defined in Ref. 8. The definitions of z_γ and z_β and the phase conventions used here correspond to those in Refs. 8, 9, and 26. In terms of the values of $B_g = B(E2; 0_g^+ \to 2_g^+)$, $B_\gamma = B(E2; 0_g^+ \to 2_\gamma^+)$, and $B_\beta = B(E2; 0_g^+ \to 2_\beta^+)$, the ratios of the intrinsic $E2$ matrix elements can be obtained from the following equations:

$$\frac{Q_\gamma}{Q_g} = \frac{1}{\sqrt{2}\,(1 - z_\gamma)} \left(\frac{B_\gamma}{B_g}\right)^{1/2} \tag{37}$$

and

$$\frac{Q_\beta}{Q_g} = \frac{1}{1 - 6\bar{z}_\beta} \left(\frac{B_\beta}{B_g}\right)^{1/2}. \tag{38}$$

The ratio $R(22, 02)$ can be written in the form (assuming $\delta R_m = 0$)

$$R(22, 02) = 1 - 3\frac{B_\gamma}{B_g} \frac{z_\gamma}{(1 - z_\gamma)^2} + 6\frac{B_\beta}{B_g} \frac{\bar{z}_\beta}{(1 - 6\bar{z}_\beta)^2} \tag{39}$$

and the isomer shift is given by[8]

$$\frac{\delta\langle r^2\rangle}{\langle r^2\rangle} = \frac{10}{3} \frac{I(I+1)}{Z} \rho(E0; 0_g^+ \to 0_\beta^+) \times \left(\frac{B_\beta}{B_g}\right)^{1/2} \frac{z_\beta(I, I)}{1 - 6\bar{z}_\beta(I, I)}. \tag{40}$$

As can be seen from Eq. (39), the coupling with the β band causes an increase in the ratio $R(22, 02)$, whereas the coupling with the γ band causes a decrease in this ratio. Therefore, it is possible that the effects of the β and γ mixings approximately cancel which could result in the apparent pure rotational value of $R(22, 02)$ observed for ^{152}Sm.

To investigate this possibility we have computed the value of $R(22, 02)$ for ^{152}Sm using Eq. (39) and the previously determined values of $z_\gamma = 0.09$ and $\bar{z}_\beta = 0.08$ together with B_g, B_γ, and B_β. This calculation, which is independent of the present measurements, yields $R(22, 02) = 1.004$, in excellent agreement with our experimental value. As an alternative approach, which indicates that the ratio $R(22, 02)$ is, in fact, sensitive to $\bar{z}_\beta$, we have also determined a value of $\bar{z}_\beta = 0.094^{+0.010}_{-0.034}$ from the present muonic value of $R(22, 02)$ and the previously measured values of z_γ, B_g, B_γ, and B_β.

Extending this interpretation, the ratio $R(22, 02)$ may be used together with Eq. (19) to estimate the difference δR_m of the effective quadrupole radii of the static- and transition-charge distributions. A value $\delta R_m = -0.05 \pm 0.11$ fm is obtained. This value, which is compatible with zero, serves primarily to indicate the similarity of the static 2^+ state and transitional 2^+-0^+ charge densities.

In the case of the ground-state band 2^+-0^+ isomer

shift, which is sensitive only to mixing with the β band, the β and γ mixing effects do not cancel. A calculation using the reduced transition monopole matrix element $\rho(E0;0_g^+ \rightarrow 0_\beta^+) = 0.19 \pm 0.04$ (Ref. 40) and $\bar{z}_\beta = 0.08$ in Eq. (40) yields an isomer shift $\delta\langle r^2\rangle/\langle r^2\rangle = (6.9 \pm 1.5) \times 10^{-4}$, in good agreement with experiment. It should be noted that $\rho(E0; 0_g^+ \rightarrow 0_\beta^+)$ should be used in Eq. (40) rather than $\rho(E0; 2_g^+ \rightarrow 2_\beta^+)$ which may already involve the mixing effect.

Thus, the present experimental values of $R(22, 02)$ and of $\delta\langle r^2\rangle/\langle r^2\rangle$ for ^{152}Sm and all of the experimental $B(E2)$ values can be described consistently in terms of the phenomenological RVI model. In ^{150}Sm, the larger isomer shift and the deviation of the ratio $R(22, 02)$ from unity seem to indicate a larger mixing parameter z_β than in ^{152}Sm. However, it is to be expected that Eqs. (39) and (40) are not applicable in the case of ^{150}Sm where the higher-order expansion of interaction terms may play an important role.

Among the various microscopic calculations, only Kumar[15] has presented both the $E2$ moments and isomer shifts for ^{150}Sm and ^{152}Sm. Although the Hartree-Bogoliubov calculation by Kumar[15] correctly predicts $R(22, 02) = 1$ for ^{152}Sm, it predicts $R(22, 02)$ smaller than unity for ^{150}Sm, in clear disagreement with experiment. Also, the calculated isomer shift for ^{152}Sm is much larger than the experimental value, although good agreement with the experimental isomer shift was found for ^{150}Sm.

Although the boson-expansion calculation[16] predicts values of $R(22, 02)$ in agreement with experiment for both of the nuclei, no isomer shifts were presented in this work. Meyer and Speth[41] have calculated the isomer shift for ^{152}Sm taking into account the Coriolis antipairing effect and obtained good agreement with experiment. However, no nuclear quadrupole parameters were calculated in their work. Hence, at present no single microscopic nuclear model seems to describe all the known properties of the lower excited states of both ^{150}Sm and ^{152}Sm satisfactorily.

In conclusion, we note that the results of most previous theoretical calculations are quoted in terms of root-mean-square radii and point-nucleus quadrupole moments, whereas the quantities that can be determined precisely and model independently with muonic x rays are Barrett moments and generalized multipole moments. Although these latter quantities do not possess the time-honored social standing of the former, they can currently be determined with higher precision and, therefore, can provide a more stringent test of theory. To assist future theoretical comparisons, we have expressed the model-independent quantities in a form so that one can calculate these quantities from the knowledge of the nuclear wave functions alone.

Note added in proof: We have received a report [Muonic x-ray study of the charge distribution of^{144,148,150,152,154}Sm, R. J. Powers, P. Barreau. B. Bihoreau, J. Miller, J. Morgenstern, J. Picard, and L. Roussel; CALT-63-297 (unpublished)] describing an independent muonic x-ray study of the Sm isotopes. The experimental data reported by Powers *et al.* are in good agreement with those reported here. In some instances the procedures followed in analyzing the data differ in the two studies (for example, the treatment of nuclear polarization) and there are therefore some slight differences in the values of certain derived parameters.

ACKNOWLEDGMENT

The authors wish to thank G. A. Rinker and J. G. Wills for making available computer codes used in some of the calculations of this work. We would like to acknowledge many helpful discussions with H. D. Wohlfahrt.

*Supported by U. S. Department of Energy.

[1]M. Sakai, Nucl. Data A8, 323 (1970); A10, 511 (1972); M. Sakai and A. C. Rester, *ibid.* 20, 441 (1977).
[2]C. M. Baglin, Nucl. Data Sheets 18, 223 (1976).
[3]M. J. A. De Voigt, Z. Sujkowski, D. Chmielewska, J. F. W. Jansen, J. Van Klinken, and S. J. Feenstra, Phys. Lett. 59B, 137 (1975).
[4]O. Lönsjö and G. B. Hagemann, Nucl. Phys. 88, 624 (1966).
[5]R. M. Diamond, F. S. Stephens, K. Nakai, and R. Nordhagen, Phys. Rev. C 3, 344 (1971).
[6]G. Goldring and U. Smilansky, Phys. Lett. 16, 151 (1965).
[7]G. Kaspar, W. Knüpfer, W. Ebert, P. Holleczek, and N. Fiebiger, in *Proceeings of the International Conference on Nuclear Reactions Induced by Heavy Ions, Heidelburg, Germany*, edited by R. Bock and W. R. Hering (North-Holland, Amsterdam, 1970), p. 471.
[8]L. L. Riedinger, N. R. Johnson, and J. H. Hamilton, Phys. Rev. 179, 1214 (1969).
[9]I. A. Fraser, J. S. Greenberg, S. H. Sie, R. G. Stokstad, G. A. Burginyon, and D. A. Bromley, Phys. Lett. 23, 1047 (1969).
[10]E. Veje, B. Elbek, B. Herskind, and M. C. Olesen, Nucl. Phys. A109, 489 (1968).
[11]D. Hitlin, S. Bernow, S. Devons, I. Duerdoth, J. W. Kast, E. R. Macagno, J. Rainwater, C. S. Wu, and R. C. Barrett, Phys. Rev. C 1, 1184 (1970).

[12]T. Cooper, W. Bertozzi, J. Heisenberg, S. Kowalski, W. Turchinetz, C. Williamson, L. Cardman, S. Fivozinsky, J. Lightbody, Jr., and S. Penner, Phys. Rev. C 13, 1083 (1976).
[13]H. Fischer, D. Kamke, H. J. Kittling, E. Kuhlmann, H. Plicht, and R. Schormann, Phys. Rev. C 15, 921 (1977).
[14]K. Kumar, Phys. Rev. Lett. 26, 269 (1971).
[15]K. Kumar, Nucl. Phys. A231, 189 (1974).
[16]T. Kishimoto and T. Tamura, Nucl. Phys. A270, 317 (1976).
[17]M. Hoshi and Y. Yoshizawa, J. Phys. Soc. Japan 42, 1106 (1977).
[18]K. W. Ford and J. G. Wills, Phys. Rev. 185, 1429 (1969).
[19]R. C. Barrett, Phys. Lett. 33B, 388 (1970).
[20]R. Engfer, H. Schneuwly, J. L. Vuilleumier, H. K. Walter, and A. Zehnder, At. Data Nucl. Data Tables 14, 509 (1974).
[21]L. K. Wagner, E. B. Shera, G. A. Rinker, and R. K. Sheline, Phys. Rev. C 16, 1549 (1977).
[22]G. A. Rinker and R. M. Steffen, At. Data Nucl. Tables 20, 143 (1977).
[23]E. B. Shera, E. T. Ritter, R. B. Perkins, G. A. Rinker, L. K. Wagner, H. D. Wohlfahrt, G. Fricke, and R. M. Steffen, Phys. Rev. C 14, 731 (1976).
[24]D. Kessler, H. Mes, A. C. Thompson, H. L. Anderson, M. S. Dixit, C. K. Hargrove, and R. J. McKee, Phys. Rev. C 11, 1719 (1975).
[25]C. K. Hargrove, E. P. Hincks, R. J. McKee, H. Mes, A. L. Carter, M. S. Dixit, D. Kessler, J. S. Wadden, H. L. Anderson, and A. Zehnder, Phys. Rev. Lett. 39, 307 (1977).
[26]A. Bohr and B. R. Mottelson, *Nuclear Structure* (Benjamin, New York, 1969, 1975), Vols. I and II.
[27]E. A. Uehling, Phys. Rev. 48, 55 (1935).
[28]G. Källen and A. Sabry, K. Dan. Vrdensk. Selsk. Mat.-Fys. Medd. 29, No. 17 (1955).
[29]L. W. Fullerton and G. A. Rinker, Phys. Rev. A 13, 1283 (1976).
[30]J. M. McKinley (unpublished). An explicit form of this correction is presented in A. Zehnder, F. Boehm, W. Dey, R. Engfer, H. K. Walter, and J. L. Vuilleumier, Nucl. Phys. A254, 315 (1975).
[31]G. A. Rinker and J. Speth (to be published).
[32]G. A. Rinker, computer code RURP, Comp. Phys. Comm. (to be published).
[33]J. M. McKinley, Phys. Rev. 183, 106 (1969).
[34]J. Johnson and R. A. Sorensen, Phys. Rev. C 2, 102 (1970).
[35]H. Backe, R. Engfer, E. Kankeleit, R. Link, R. Michaelsen, C. Petitjean, L. Schellenberg, H. Schneuwly, W. U. Schröder, J. L. Vuilleumier, H. K. Walter, and A. Zehnder, Nucl. Phys. A234, 469 (1974).
[36]Min-yi Chen, Phys. Rev. C 1, 1176 (1970).
[37]Y. Yamazaki, H. D. Wohlfahrt, E. B. Shera, M. V. Hoehn, and R. M. Steffen (to be published).
[38]F. Boehm and P. L. Lee, At. Data Nucl. Data Tables 14, 605 (1974).
[39]R. G. Stokstad, J. S. Greenberg, I. A. Fraser, S. H. Sie, and D. A. Bromley, Phys. Rev. Lett. 27, 748 (1971).
[40]N. A. Voinova, Nucl. Data Tables A11, 299 (1973).
[41]J. Meyer and J. Speth, Nucl. Phys. A203, 17 (1973).
[42]J. W. Negele and G. Rinker, Phys. Rev. C 15, 1499 (1977).
[43]H. Flocard, P. Quentin, and D. Vautherin, Phys. Lett. 46B, 304 (1973).